# Membrane Separation Process Design and Intensification

Salih Emre Demirel, Jianping Li, and M. M. Faruque Hasan\*

Artie McFerrin Department of Chemical Engineering, Texas A&M University

College Station, TX 77843-3122, USA

#### Abstract

Membrane separation has gained significant interest from the chemical industry due to their compactness, energy efficiency, and modularity. Recent trends in process intensification also emphasizes the importance of more widespread adoption of membrane-based processes for significant cost savings and sustainable operation. We present a prototype software framework for the automated design, optimization, intensification, benchmarking, and technoeconomic analysis of various types of membrane systems, including gas separation, pervaporation and vapor permeation, while covering wide ranges of their operations. The framework is based on a generic building block-based representation (Demirel, Li, and Hasan, Comput. Chem. Eng., 2017, 150, 2 - 38) that can be used for automated process synthesis and screening of numerous designs for selecting optimal membrane modules, processes and network configurations. We can also generate rank-ordered lists of optimal process flowsheets based on different objectives. We present several case studies to demonstrate the utility of the proposed approach and report substantially better solutions compared to the designs reported in the literature.

**Keywords**: Membrane Network Synthesis, Process Synthesis, Process Intensification, Building block superstructure

<sup>\*</sup>Correspondence concerning this article should be addressed to M.M. Faruque Hasan at hasan@tamu.edu, Tel.: 979-862-1449.

### 1 Introduction

Almost all industrial chemical processes involve separating mixtures into pure components. Chemical separation is not a spontaneous process and, therefore, requires external energy supply. In fact, 10–15% of the world's energy consumption is attributed to separation processes, such as distillation. Chemical separations also account for half of U.S. industrial energy use. Membrane technologies have shown potential to offer alternative solutions to several energy-intensive separations. Owing to their high efficiency, compactness and modularity, membranes and related processes have been widely investigated for separating gases and liquid mixtures in the chemical process industry (CPI). Gas separation membranes have been developed for air separations, hydrogen recovery, carbon capture, acid gas removal from natural gas, olefin-paraffin separations, and other applications. More than one hundred pervaporation membrane processes are reported for solvent dehydration alone.

Membranes are also used to enhance the performance of other technologies. Examples include, but are not limited to, chemical transformations in membrane reactors, proton exchange membrane fuel cells, reverse osmosis-driven water purification, and hybrid separations using membrane contactors. Pala A modular system consists of modules with few connectivity so that difficult module assembly tasks can be performed offsite. Beach module has one or more equipment units, which can be further intensified. Intensification refers to drastic improvement in process performance in terms of cost, energy consumption, size, waste, etc. Due to their modular and compact designs, membrane processes are excellent candidates for modular chemical process intensification (MCPI). The versatile use of membranes brings new opportunities for synergistic integration of separation and/or reaction phenomena in multifunctional units (e.g., membrane distillation and membrane reactors), thus leading to substantial improvements in equipment size, efficiency, energy, investment, environmental impact, and process safety.

To realize the full potential of membrane materials, we need systematic methods

incorporating membranes at the conceptual process design stage.<sup>21</sup> There have been significant efforts in the past in terms of systematic modeling, simulation, synthesis and optimization for membrane process development. <sup>22–31</sup> For example, Marriott et al. <sup>32</sup> introduced a detailed 2D mathematical model to predict the performance of a hollow-fiber membrane module. Tessendorf et al.<sup>33</sup> proposed a computational framework for designing gas separation membrane systems. Pathare and Agrawal<sup>34</sup> enumerated and simulated all feasible cascade configurations of interest and studied membrane cascade designs with varying number of stages for binary gas separation. Hasan et al.<sup>25</sup> employed nonlinear programming (NLP) for the optimal design of multistage membrane processes to separate  $CO_2$  from multicomponent flue gas mixtures. Zarca et al. 35 also used NLP to optimize multistage olefin/paraffin membrane separation processes. Aliaga-Vicente et al. <sup>36</sup> and Ohs et al. <sup>37</sup> employed mixed integer nonlinear programming (MINLP) to optimize membrane cascade for gas separation. Recently, Eugene et al. 38,39 performed modeling and superstructure optimization of membrane systems considering both membrane property and process design targets. Significant works also exist in designing multistage membrane configurations. 25,36,40,41 However, there are few works that provides generic platforms for the design and optimization of membrane-based processes. Uppaluri and Linke $^{42}$  used a superstructure-based process synthesis approach to screen optimal membrane networks. The state-space representation, which was originally developed for synthesizing mass-exchange networks, <sup>43</sup> can be also used for membrane networks synthesis. An example is the synthesis of pervaporation membrane networks for waste reduction. 44 Bounaceur et al. 45 proposed MEMSIC, which employs finite difference discretizations to consider pressure-dependent variable permeabilities while simulating gas separation membranes. Recently, Mohammadi et al. (2020) developed OMPD (Optimal Membrane-Process Design), which is a design tool based on a genetic algorithm-based approach to generate different membrane process configurations for gas separation applications. 46

Membrane-based process design activities include the selection of single or multiple

membrane modules and auxiliary equipment, identification of optimal design and operating conditions for each module to achieve a desired separation performance, and optimal sequencing or arrangement of membrane modules in a process flowsheet. Recent advances in computer-aided process synthesis and intensification methodologies (see recent reviews <sup>47,48</sup>) can be leveraged to achieve these. Process synthesis methods often employ the so-called "superstructures" that contain many connectivities and pathways representing different process configurations or flowsheets. This approach is computationally powerful, since it allows cutting-edge discrete/continuous optimization-based techniques (e.g., MINLP) to efficiently screen the optimal designs. The effectiveness of process synthesis, however, largely depends on the rigor and the full connectivity of the superstructure used. In most cases, one spends significant time to formulate a superstructure with many distinctly possible configurations to enrich the search space.

In this work, we present a systematic process design and synthesis approach for membrane separation processes. Given the feed and product specifications, membrane properties and techno-econo-environmental parameters and constraints, this paper describes how we can utilize the generic "building block" approach, originally developed for the systematic design and intensification of chemical process systems, <sup>18,49-51</sup> to develop, screen and optimize membrane-based processes. The building block approach uses only two fundamental design elements, namely the blocks and the boundaries. This allows to systematically generate and optimize numerous membrane modules and process configurations. The implementation of this approach is such that it requires the feed composition, product specifications (e.g., recovery, purity), and the membrane properties. Depending on the membrane type and problem requirements, physical properties (e.g., heat capacity) and economic parameters (e.g., unit capital and operating costs) might be also needed. Given this information the approach automatically generates screens and optimizes the stop conceptual designs.

Unlike most studies that either design either at the material-, module-, or process-level, our building block is a generic approach that has the capability to perform sequential/simultaneous designs at all three levels. At the membrane level, we can perform regular assimilation of membrane performance. At the modular level, we can perform the design and configuration of membrane modules with different flow arrangements (e.g., cocurrent or countercurrent, sweep gas, membrane reactors, etc.). At the process and network levels, we can identify the optimal sequence and arrangement of different membrane modules for desired separation performance while minimizing the cost and energy penalty. We can also generate rank-ordered list of optimal process flowsheets based on different objectives. The approach is not only limited to membrane separation but it can also be applied to benchmark with other separation processes, such as distillation and absorption. Furthermore, unlike the most recent state-of-the art software frameworks available in the literature, <sup>46</sup> current work does not need simplifying assumptions on module design and can be readily integrated into process synthesis <sup>52</sup> and intensification. <sup>49-51</sup> Lastly, it can be used to generate hybrid separation schemes that may include multiple separation phenomena (e.g., membrane, distillation or both).

We organize the paper as follows. In section 2, we provide a description of the building block representation and how it is used for membrane-based operations. In section 3, we describe the mathematical model that is used to synthesize optimal membrane process configurations. We then illustrate the framework using case studies in Section 4 before providing some concluding remarks in Section 5.

# 2 Building Block Representation

Building blocks are abstract modules that can be used to represent many different chemical phenomena, task and equipment. Various interactions between these building blocks result in many types of traditional and intensified equipment and flowsheets. A more detailed description on how different chemical phenomena can be represented through building blocks can be found in our previous works. <sup>49–52</sup> Here, we provide the specifics on how to apply this novel representation for the synthesis of different membrane-based separation processes.

Building blocks are two-dimensional abstract modules characterized by their interiors and surrounding four boundaries (See Figure 1a-i). While the block interior is used to represent functional materials such as catalysts, etc., block boundaries are used to describe the interaction between neighboring blocks. The block boundaries are classified into three types: (i) unrestricted boundary, (ii) semi-restricted boundary, and (iii) completely restricted boundary (Figure 1a-ii). Unrestricted boundary indicates an interaction that is not restricted with any mass transfer limitations. Semi-restricted boundary represents a mass transfer interception. It can either emulate an interphase between two phases that are in direct contact with each other, or represent a barrier material that facilitates selective mass transfer. A membrane is an example of a barrier material. Completely restricted boundary prevents any material transfer across itself and, therefore, represents zero flow, e.g. dividing walls.<sup>53</sup> Each block can have inlet and outlet streams through its four boundaries for material and energy transfer. External feed streams and product withdrawals are also allowed to enable interaction with outside of the overall process system. Energy in the form of heat and work can flow in or taken out through utility streams.

Each building block has temperature (T), pressure (P), and a set of composition variables  $(y_k)$ , where k represents a chemical species in a mixture. The phase of the chemical mixture in a block is determined based on these attributes using an appropriate thermodynamic model. Furthermore, each stream has the same temperature and pressure of its source block. The chemical compositions of interblock streams depend on the boundary types. If the boundary is unrestricted, then the stream that passes through it has the same composition of its source block. If the boundary is semi-restricted, then the composition is determined based on the nature of driving force for mass transfer. For membranes, this is governed by Fick's law or Darcy's law.

By using these building block and boundary features and combining them in a certain fashion, we can represent many different physicochemical phenomena that exist in the chemical process industry (Figure 1b). Mixing and splitting of material streams of the same

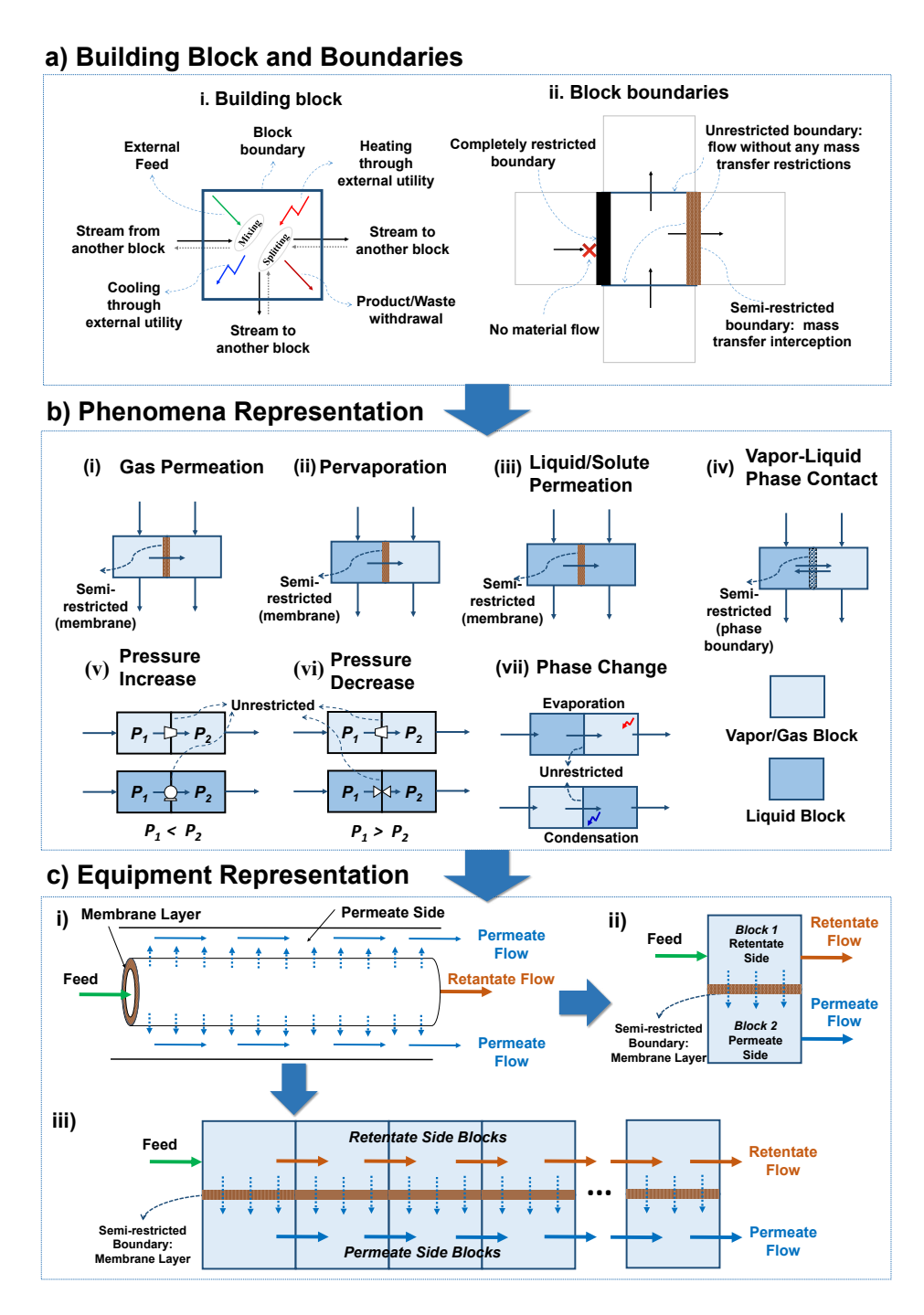


Figure 1: a) Each building block can have entering and outgoing streams through its boundaries and external feed and product streams and interaction between different blocks are realized through three different boundary types, b) representation of different phenomena by using building blocks that are required for membrane-based separation processes, c) using these phenomena descriptions many different membrane configurations can be represented with varying detail. Here, c-i) represents a part of a membrane module, c-ii) shows the representation when complete mixing is assumed at both permeate and retentate sides and a short-cut model is used to describe the module and c-iii) shows a more intricate representation capturing the plug flow behavior by combining multiple building blocks.

phase can be represented through a single block with multiple inlet and outlet streams. When multiple streams enter into a block, they are assumed to be completely mixed before leaving the block. Heating and cooling can be also achieved through a single block with external utilities. By assigning different membrane materials and block phases, we can represent all the major types of membrane operations. For example, gas or vapor permeation phenomena observed in gas separation and vapor permeation membranes can be represented by using two building blocks in gas/vapor phases separated through semi-restricted boundary which stands for the membrane material (Figure 1b-i). Similarly, liquid or solute permeation that takes place in reverse osmosis operations can be represented by two liquid blocks separated through the semi-restricted boundary (Figure 1b-iii). Pervaporation operations on the other hand are represented through building blocks of different phases, one in liquid and the other in vapor phase (Figure 1b-ii). In a similar manner, these building blocks can be used to represent other membrane operations including membrane absorption with the gas phase and liquid absorbent positioned at the opposite sides of the boundary. In representing building blocks for membrane operations, the permeate or retentate sides are determined according to the direction of the permeating stream. In Figure 1b, all the semi-restricted streams flow towards the right direction, hence, the block on the left stands for the retentate and the block on the right stands for the permeate side. Semi-restricted boundary can be also used to represent the direct contact between two different phases. An example is vapor-liquid phase contact that can be observed in distillation or flash operations (Figure 1b-iv). In this case, semi-restricted flows are used to represent the mass transfer between the two phases. Pressure manipulations (Figure 1b-v and 1b-vi) are realized through equipment positioned on the unrestricted streams. These can include compressors, vacuum pumps, expanders, valves, etc. Finally, complete phase transfer between different phases are represented through two blocks connected through unrestricted boundary (Figure 1b-vii). The boundary is unrestricted as the composition does not change as a result of complete phase transition.

Based on these phenomena representations using building blocks, one can be generate and

analyze many different membrane operations. An illustrative example operation is shown in Figure 1c. A part of the membrane module is depicted in Figure 1c-i which features a co-current flow between permeate and retentate sides. This can be represented through building blocks in at least two different ways. If one assumes complete mixing at both the permeate and retentate sides, then using only two blocks separated by a semi-restricted boundary with a membrane layer is sufficient to emulate the overall separation performance (Figure 1c-ii). However, it is also possible to achieve a plug flow regime and observe each building block pair as a differential flow element. In this case, multiple building blocks connected in series can be used to represent the membrane operation, as shown in Figure 1c-iii. Other intricate features can be also considered.

The building blocks inherently allow a multi-scale approach for the synthesis of membrane modules. For instance, if one describes the flow through semi-restricted boundaries with a mass transfer model accounting for the internal and external mass transfer resistances, then it can be utilized as a finite element approach for modeling and each block can serve as an approximation for the spatial coordinates. This can be used to simulate or optimize the design of a single hollow fiber, a tube, or a single sheet of the membrane module. If one neglects the interphase phenomena or considers a lumped mass transfer coefficient, then each two neighboring block separated through a semirestricted boundary can be used to represent a part of a membrane module and combination of these can be used to describe the flow behaviour in the whole module. If one considers a short-cut model with complete mixing assumption (or uses log-mean concentration differences as discussed in the modeling section), on the other hand, then these two blocks represent the whole membrane operation. This provides a multi-scale representation approach for the synthesis of membrane operations.

To select and combine these building blocks in a systematic manner, we collect them in a two-dimensional grid as shown in Figure 2a and obtain building block superstructure. Each block within the grid is denoted as  $B_{i,j}$ , where i = 1, ..., I is for the rows, j = 1, ..., J is for the columns. Connection between the blocks are facilitated through interblock streams which can

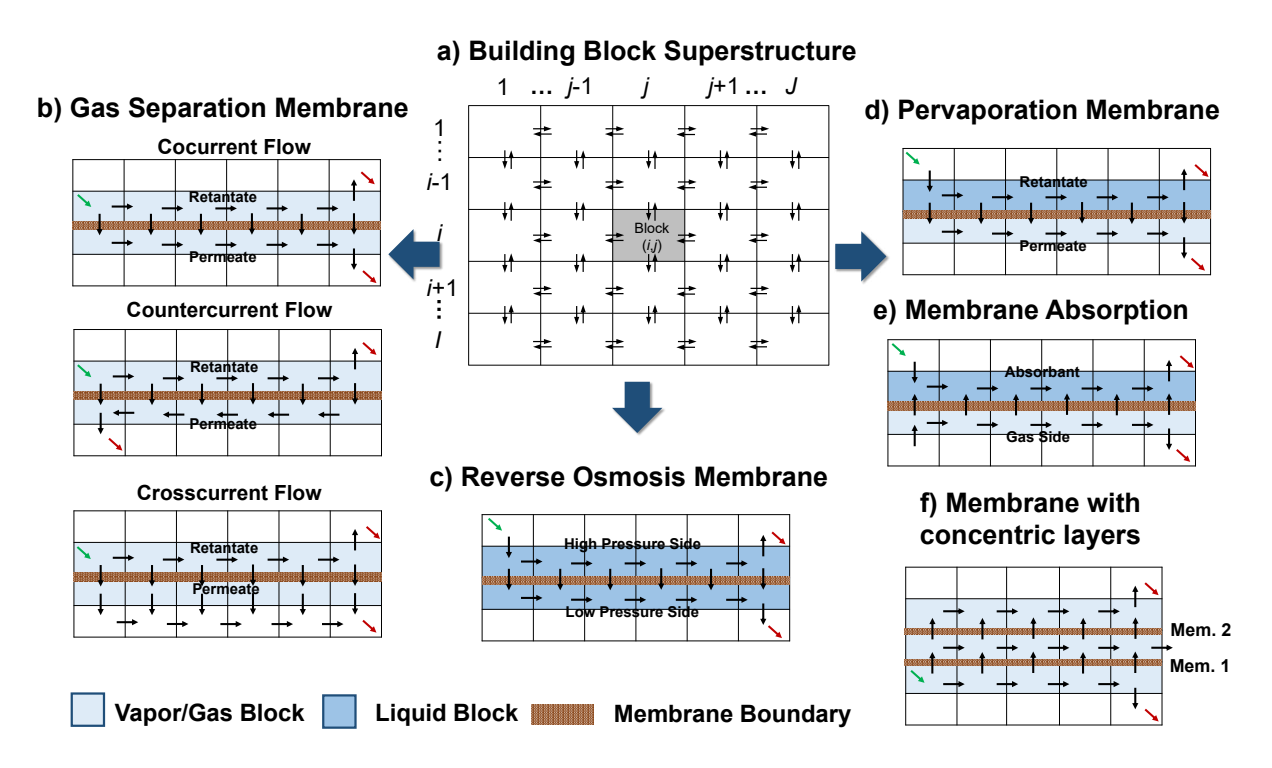


Figure 2: From the same superstructure, many different membrane-based processes with different flow patterns can be generated. a) Building block superstructure, b) gas separation membrane representation with cocurrent, countercurrent and crosscurrent flow patterns, c) reverse osmosis representation, d) pervaporation membrane representation (or membrane distillation), e) membrane absorption representation (by changing the permeate flow direction, membrane stripping can be also captured), and f) a membrane module representation comprised of two concentric tubes.

flow in either forward or backward direction. From this generic superstructure representation, by changing the phase, boundary types, flow directions and membrane types, different membrane operations with many different configurations can be obtained. For instance, two arrays of blocks with gaseous mixtures separated by a semi-restricted boundary representing the membrane material can be used to obtain a gas separation membrane module (Figure 2b). The function of the block, i.e. retentate or permeate side, is determined according to the direction of the semi-restricted flow. Different flow patterns can be also captured via changing the flow directions in the permeate or retentate side of the blocks for the module. Counter-current, co-current and cross-current flow patterns can be all captured. If both sides of the membrane boundary are in liquid phase and the retentate mixture contains a solute,

then a reverse osmosis or dialysis membrane can be obtained as shown in Figure 2c. Similarly, if the retentate side is fed with a liquid mixture and it changes phase across the membrane boundary, then a pervaporation membrane module can be obtained as shown in Figure 2d. Different membrane contractors can be also represented for many applications. An example on membrane absorption module is shown in Figure 2e. If the flow directions is reversed, then a membrane stripper can be also captured. Note that although the representation of these different type of membranes are similar in block-wise representation, description of the semi-restricted flow through the membrane boundaries will dictate the nature of the mass transfer. This will be discussed in the next section.

More intricate structures are also possible as shown in Figure 2f. If three different rows of blocks are connected in parallel by semi-restricted boundaries, then a membrane module with three different regions can be obtained. This might stand for a membrane module with concentric tubes with permeable walls. Here, the fresh feed enters into the innermost tube. By changing the direction of the semi-restricted flows, feed positions and direction of the horizontal streams across the rows, many other eccentric configurations can be obtained from the same superstructure representation. While these structures are mostly investigated by ad hoc basis, this representation enables a systematic tool for the design and synthesis of such structures at the conceptual design stage.

Often times single membrane modules are not sufficient to realize the separation targets. As a remedy, multi-stage modules with parallel/series arrangements are used. Building block representation can be also used to capture these different configurations and construct different membrane networks. This can be performed by designating several regions within the superstructure for alternative membrane modules and connecting them through interblock connections to capture different recycle connections, e.g. retentate-retentate. While building these connections, just utilizing the connections between the interblock streams might not be sufficient. Hence, we also use "jump streams" that can connect non-adjacent blocks to each other. These streams provide flexibility and enable to build

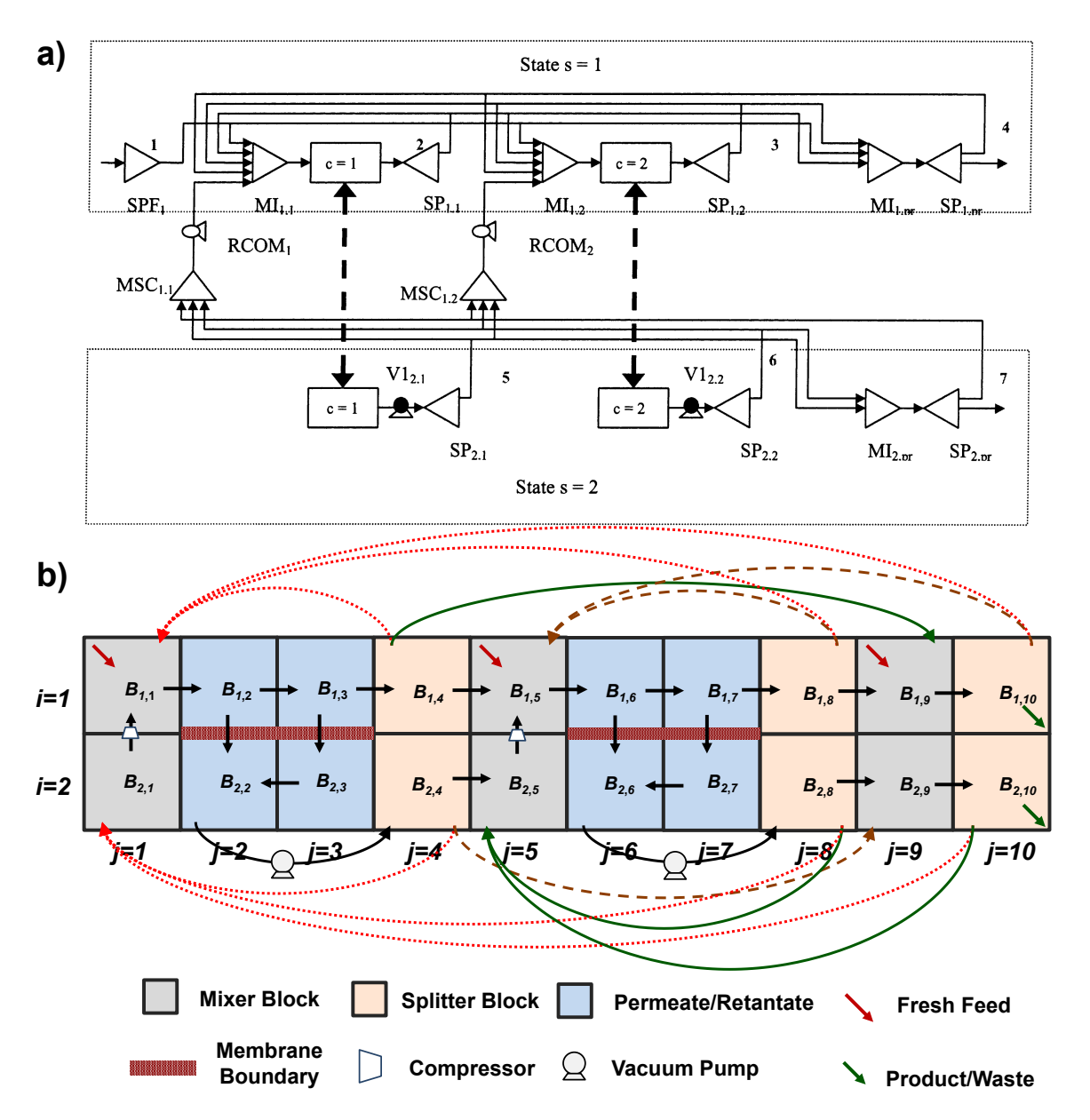


Figure 3: A gas separation membrane network superstructure example taken from Uppaluri et al. (2004).<sup>42</sup> a) Original superstructure representation (Figure is reprinted with permission from (Uppaluri, R.V., Linke, P. and Kokossis, A.C., 2004. Synthesis and optimization of gas permeation membrane networks. Industrial & engineering chemistry research, 43(15), pp.4305-4322.). Copyright (2004) American Chemical Society), b) building block representation of the same superstructure.

superstructures with full connectivity.<sup>54</sup> A gas separation membrane network superstructure with two membrane modules taken from literature is shown in Figure 3a.<sup>42</sup> Uppaluri et al. (2004) considers retentate-retentate, permeate-retentate and feed splitting connections and

divides the permeate and retentate sides into several compartments to imitate the plug flow behaviour. In Figure 3a, these compartments are not shown. In Figure 3b, building block representation for the same superstructure is demonstrated with a superstructure of size  $2\times10$  with I=2 and J=10. Here, we used two compartments to show countercurrent flow pattern for each membrane module for simplicity, but number of blocks can be increased to improve the model accuracy as it will be shown in the case studies. Similarly, permeate side flow directions can be modified as shown in Figure 2 to simulate different flow regimes. In Figure 3a, there are two membrane modules. The first one is represented by the blocks  $B_{1,2}, B_{1,3}, B_{2,2}$  and  $B_{2,3}$ . While the two blocks on the first row represent the retentate side, the two blocks on the second row represent the permeate side. Similarly, the second membrane module is represented through blocks  $B_{1,6}, B_{1,7}, B_{2,6}$  and  $B_{2,7}$ . On the retentate side, the first row of the block superstructure, we have mixer  $(B_{1,1}, B_{1,5}, B_{1,9})$  and splitter blocks  $(B_{1,4}, B_{1,8}, B_{1,10})$  to capture the recycle connections. To illustrate, the retentate of the second membrane module is taken to splitter in  $B_{1,8}$  where it can be distributed to inlet mixer of the first module, block  $B_{1,1}$ , inlet mixer of the second module, block  $B_{1,5}$ , or it can be taken into retentate product mixer block  $B_{1,9}$ . Note that while the last connection here is built through an interblock stream, the other two are achieved through jump streams (shown as curved arrows on Figure 3b). After this mixing at the product mixer block  $B_{1,9}$ , components are taken to block  $B_{1,10}$  which serves as the product splitter block. Here, product stream can be either taken out from the superstructure or some fraction of it can be sent back to the membrane inlet mixers. Note that feed splitting is represented through allowing different fractions of the available fresh feed to be sent for the mixer blocks (Red diagonal arrow on the left corners). Similar connections also exist in the second row which depicts the permeate side and the corresponding connections. Here, the reference work does not consider any permeate-permeate connections, hence, they are not shown. Here, blocks  $B_{2,1}$  and  $B_{2,5}$  depict the mixers for the permeate-retentate recycle streams. Outlet from these blocks are sent to the retentate inlet mixers after they are compressed to the retentate pressure. Membrane permeate streams, depicted as jump streams, are embedded with vacuum pumps to account for the cost of achieving sub-atmospheric pressures. All the permeate outlet streams are sent to permeate product mixer block at  $B_{2,9}$ . From this block, mixture is sent to the permeate product splitter at  $B_{2,10}$ . Here, either the product stream can be taken out of the process or it can be sent back to the retentate side through  $B_{2,1}$  and  $B_{2,5}$ .

Here, we have shown an example with two membrane modules considering two compartments per module with series arrangement. However, this representation can be easily generalized as a generic superstructure representation for problems with more number of modules and alternatives. Then one can just state the number of compartments used in representing the modules and the maximum number of modules needed in the process to obtain the corresponding superstructure automatically. This is done by following a set of rules for deciding on the position of the membrane boundaries, mixers, splitters, feed and product blocks which ultimately determine the required building block superstructure size, namely I and J. For example, for the superstructure example taken from Uppaluri et al. (2004), if we denote the number of modules with  $n^{module}$  and compartments in each module with  $n^{comp}$ , one would need I=2 rows and  $J=n^{module}\times(n^{comp}+2)+2$  columns to construct the superstructure. This is determined as follows: One needs mixer and splitter blocks before and after each membrane module to allow different permeate and retentate recycle connections. In between these mixer and splitter blocks, membrane boundaries can be positioned. The number of boundaries required is determined by the number of compartments used to represent the module, i.e.  $n^{comp}$ . This indicates that for each membrane module at least  $n^{comp} + 2$  neighboring blocks are needed including mixers and splitters. To represent a membrane, we need at least two separate rows of blocks for permeate and retentate sides. Accordingly, we can specify the number of rows as: I=2. If we had parallel structures, more rows could be considered. Each parallel configuration can be built as two additional rows and connections in between can be realized through jump streams. Another way to consider parallel arrangements would be to allow product/waste streams from each splitter block. Accordingly, each membrane module with its mixers and splitters requires I=2 rows and  $J=n^{comp}+2$  columns. This is multiplied with the maximum number of membrane modules to obtain the number of columns needed for the membrane modules and their connections:  $n^{module} \times (n^{comp}+2)$ . Two additional columns of blocks are also considered at the right end of the superstructure as product/waste mixer and splitter blocks. This results in the above-mentioned formula for the superstructure size determination.

While this shows that building block representation can be used as a generic superstructure representation method for membrane-based processes, another novel feature is that it can be also used to automatically generate the membrane-based processes without requiring any specifications over the membrane flow patterns, number of modules, recycle patters or stage arrangements beforehand. This is achieved by not designating the position of the membrane boundaries and flow directions beforehand, but allow them to be variables for an optimization problem. This allows each boundary within the grid to be assigned with the membrane boundary, each stream through the boundaries be either unrestricted, semirestricted or completely restricted and each stream to flow in either forward and backward direction. This is facilitated through a Mixed-Integer Nonlinear Programming Model as it will be shown in the next section. This MINLP model also provides a generic mathematical representation for the building block superstructure from which sub-models can be also derived for different membrane network superstructures.

### 3 Mathematical Model

In this section, a general MINLP model for the synthesis of membrane systems is provided. The model is based on Demirel et al. (2017).<sup>49</sup> Here, we provide a description on how it can be utilized for the synthesis of membrane-based separation systems with several additional features. One important feature of the model is that it allows for automated generation of intensified process flowsheets via allowing any phenomena included in the solution space to be assigned to any position in the superstructure. Furthermore, this general model

can be reduced to represent a limited number of alternatives which enables to construct superstructures for synthesis of intensified and/or traditional membrane networks.

### 3.1 Problem Description

Given a set  $K = \{k|k = 1, ..., |K|\}$  of chemical species, a set  $FS = \{fs|fs = 1, ..., |FS|\}$  of raw material/feeds streams with their maximum availability  $F_{fs}^{feed}$  and composition,  $y_{k,fs}^{feed}$ , a set  $S = \{s|s = VP, PV, GP, LP, ..., |S|\}$  of permeation related phenomena with different phase and driving force constraints, a set  $M = \{m|m = 1, ..., |M|\}$  of membrane materials that can include materials for vapor permeation, pervaporation, osmosis, membrane absorption, etc., the goal is to design a membrane process that minimizes/maximizes a set objectives, e.g. minimize total annual cost, and produces a set  $PS = \{ps|ps = 1, ..., |PS|\}$  of products streams while satisfying their demand  $D_{ps}$ , minimum purity,  $y_{k,ps}^{MIN,prod}$ , and/or maximum waste/emission,  $y_{k,ps}^{MAX,prod}$ , requirements. Given is also the elements of subset  $SM \subset S \times M$  denoting the permeation phenomena s for each membrane material m. Here, VP,PV,GP and LP stand for vapor permeation, pervaporation, gas permeation and liquid permeation phenomena, respectively.

## 3.2 Optimization Model Formulation

We first summarize several generic constraints that are needed when using building superstructure. These include block material and energy balances, determination of flow directions and boundary formulations. Then, we provide a detailed description on how the membrane-based separations can be modeled with building block-based approach.

**Material Balances**: Each block and boundary variable are denoted by their position within the superstructure. Interblock flow variables  $F_{i,j,k}$  and  $R_{i,j,k}$  represent the mass flow of component k in the horizontal and vertical direction, respectively. Each of these flow variables can be in either forward or backward direction. A positive  $F_{i,j,k}$  denotes horizontal flow in forward direction from block  $B_{i,j}$  to  $B_{i,j+1}$ . A negative  $F_{i,j,k}$  indicate that the flow is

in the opposite direction, i.e., from block  $B_{i,j+1}$  to  $B_{i,j}$ . Similarly, vertical flow  $R_{i,j,k}$  in the forward direction is indicated with a positive value when the flow is from block  $B_{i,j}$  to  $B_{i+1,j}$ . When it is negative, the flow direction is from  $B_{i+1,j}$  to  $B_{i,j}$ . Fresh streams fs can enter into the superstructure at any block  $B_{i,j}$  with a rate measured by  $M_{i,j,k,fs}^{feed}$ . This represents the flow rate of component k in feed stream fs fed into the block  $B_{i,j}$ .  $H_{i,j,k,ps}$  represents the flow rate of component k in product stream ps withdrawn from block  $B_{i,j}$ . To increase connectivity within the superstructure, we also consider jump streams. We denote these streams as  $J_{i,j,i'j',k}$  where  $i = \{1,...,I\}$ ,  $j = \{1,...,J\}$ ,  $i' = \{1,...,I\}$ ,  $j' = \{1,...,J\}$  and  $k \in K$ . This represents flow of component k from block  $k_{i,j}$  to  $k_{i',j'}$ . These streams are mainly used to enable connections between non-adjacent blocks. With these, we can write the following steady-state molar balance for each component that enters and exits a block  $k_{i,j}$ :

$$F_{i,j-1,k} + R_{i-1,j,k} - F_{i,j,k} - R_{i,j,k} + G_{i,j,k} + \sum_{fs \in FS} M_{i,j,k,fs}^{feed} - \sum_{ps \in PS} H_{i,j,k,ps} + \sum_{(i',j') \in LN} J_{i',j',i,j,k} - \sum_{(i',j') \in LN} J_{i,j,i',j',k} = 0, \quad \forall i, j, k$$

$$(1)$$

$$F_{i,j=J,k} = R_{i=I,j,k} = 0. (2)$$

The flow variables in Eq. 2 are fixed to zero because we do not allow any flow at the superstructure boundaries. Similarly, all the variables associated with boundaries can be fixed to be zero. For simplicity, we will not specifically mention all of these fixed variables in the remainder of the discussion but if a variable is defined for the block boundaries, they are not needed at the superstructure borders. Note that while jump streams can be allowed between all the blocks within the grid, this would increase the model size and symmetry significantly. Hence, they are used only when necessary with subset LN(i, j, i', j') describing the active connections.  $G_{i,j,k}$  represents the amount of component k generated/consumed by a reaction. If this term is included in the model with an appropriate rate description, then reactive membrane operations can be also considered. In this work, we take  $G_{i,j,k} = 0$  and do not consider any reaction between the components included in the system.

For the feed streams, we also write the following to specify an upper bound on the fresh resources that can be fed into the system:

$$M_{i,j,k,fs}^{feed} = F_{fs}^{feed} y_{k,fs}^{feed} z_{i,j,fs}^{feedfrac}, \ \forall \ i,j,k,fs$$
 (3)

$$0 \le \sum_{i \in I} \sum_{j \in J} z_{i,j,fs}^{feedfrac} \le 1, \ \forall \ fs$$
 (4)

Here,  $F_{fs}^{feed}$  is the upper bound on the total supply of feed fs. This can be supplied into only one block or it can be distributed to multiple blocks indicating feed splitting.  $z_{i,j,fs}^{feedfrac}$  denotes the fraction of the external feed fs fed to block  $B_{i,j}$ . If all the feed fs needs to be separated, this constraint is modified as an equality:  $\sum_{i \in I} \sum_{j \in J} z_{i,j,fs}^{feedfrac} = 1$ . Product specifications are satisfied via the following:

$$y_{k,ps}^{MIN,prod} \sum_{k' \in K} H_{i,j,k',ps} \le H_{i,j,k,ps} \le y_{k,ps}^{MAX,prod} \sum_{k' \in K} H_{i,j,k',ps}, \ \forall \ i,j, \ (k,ps) \in \ kps$$
 (5)

where, the parameters  $y_{k,ps}^{MIN,prod}$  and  $y_{k,ps}^{MAX,prod}$  denote the minimum and maximum purity specifications, respectively, for component k in product ps. kps is a subset of  $K \times PS$  and it denotes the chemical component and product stream pairs with purity specifications, i.e.  $y_{k,ps}^{MIN,prod} > 0$  and/or  $y_{k,ps}^{MAX,prod} < 1$ . Demand and maximum emission constraints on product ps are ensured through the following:

$$D_{ps}^{min} \le \sum_{i \in I} \sum_{i \in J} \sum_{k \in K} H_{i,j,k,ps} \le D_{ps}^{max}, \quad ps \in PS$$
 (6)

We also define the following binary variables for feed and product streams in case constraints on feed and product positions are needed (e.g. no feed into the permeate side of a membrane):

$$z_{i,j,fs}^{feed} = \begin{cases} 1 & \text{if feed stream } fs \text{ is introduced into block } B_{i,j} \\ 0 & \text{otherwise} \end{cases}$$

$$z_{i,j,ps}^{product} = \begin{cases} 1 & \text{if product stream } ps \text{ is withdrawn from block } B_{i,j} \\ 0 & \text{otherwise} \end{cases}$$

If a feed is introduced into block  $B_{i,j}$ , then that block should be a feed block:

$$z_{i,j,fs}^{feedfrac} \le z_{i,j,fs}^{feed}, \quad \forall i, j, fs$$
 (7)

Similarly, for the product binary variables:

$$\sum_{k} H_{i,j,k,ps} \le M_{i,j,ps}^{out} \ z_{i,j,ps}^{product}, \quad \forall i, j, ps$$
 (8)

where,  $M_{i,j,ps}^{out}$  is the maximum product flow rate that can be withdrawn from a block and can be described as follows (if there is no chemical reaction):

$$M_{i,j,ps}^{out} = min(D_{ps}^{max}, \sum_{k,fs} F_{fs}^{feed} \ y_{k,fs}^{feed}), \quad \forall i,j,ps$$

Flow Directions: Each flow variable  $F_{i,j,k}$  and  $R_{i,j,k}$  is dissected into two counterparts to determine their directions.  $F_{i,j,k}$  is comprised of  $FP_{i,j,k}$  for representing its positive counterpart and  $FN_{i,j,k}$  for representing its negative counterpart. Similarly,  $R_{i,j,k}$  is comprised of  $RP_{i,j,k}$  for representing its positive counterpart and of  $RN_{i,j,k}$  for representing its negative counterpart. To determine the flow direction, we define the following two binary variables:

$$z_{i,j}^{Fplus} = \begin{cases} 1 & \text{if } F_{i,j,k} \text{ is from left to right} \\ 0 & \text{otherwise} \end{cases}$$

$$z_{i,j}^{Rplus} = \begin{cases} 1 & \text{if } R_{i,j,k} \text{ is from top to bottom} \\ 0 & \text{otherwise} \end{cases}$$

A stream can have only one direction. Accordingly:

$$F_{i,j,k} = FP_{i,j,k} - FN_{i,j,k}, \quad \forall i, j, k$$

$$\tag{9}$$

$$FP_{i,j,k} \le FU_{i,j,k} \ z_{i,j}^{Fplus}, \quad \forall i, j, k$$
 (10)

$$FN_{i,j,k} \le FU_{i,j,k} \left(1 - z_{i,j}^{Fplus}\right), \quad \forall i, j, k$$
 (11)

This unidirectional flow requirement can be relaxed for certain cases in which different components can move in reverse direction (See Demirel et al. (2017) for a discussion<sup>49</sup>). Similar constraints are valid in the vertical direction:

$$R_{i,j,k} = RP_{i,j,k} - RN_{i,j,k}, \quad \forall i, j, k$$
(12)

$$RP_{i,j,k} \le RU_{i,j,k} \ z_{i,j}^{Rplus}, \quad \forall i, j, k$$
 (13)

$$RN_{i,j,k} \le RU_{i,j,k} \left(1 - z_{i,j}^{Rplus}\right), \quad \forall i, j, k$$
 (14)

Energy Balances: Pressure and temperatures of the block  $B_{i,j}$  are denoted as  $P_{i,j}$  and  $T_{i,j}$ , respectively. Temperature and pressure of a stream is the same as its source block. The enthalpy carried by a material stream is dependent on the flow rate, temperature, pressure and the composition of the stream. Here, we dissect the enthalpy of each stream through a boundary into four parts according to its direction and the phase of its source block. The enthalpy of the stream in horizontal (vertical) direction flowing in the forward direction these terms are denoted as  $EFP_{i,j,k}^g$  ( $ERP_{i,j,k}^g$ ) for the gas/vapor phase and  $EFP_{i,j,k}^l$  ( $ERP_{i,j,k}^l$ ) for the liquid phase. In the backward direction they are defined as  $EFN_{i,j,k}^g$  ( $ERN_{i,j,k}^g$ ) for the gas/vapor phase and  $EFN_{i,j,k}^l$  ( $ERN_{i,j,k}^l$ ) for the liquid phase. Similar terms are also defined for the jumps streams. For the feed and product enthalpies, the phase is already specified in the problem definition. Hence, feed enthalpy into a block is defined as  $EM_{i,j}$  and product enthalpy is defined as  $EP_{i,j}$ . Accordingly, general block energy balance can be written as

follows:

$$\sum_{k \in K} EFP_{i,j-1,k}^{g} + \sum_{k \in K} EFP_{i,j-1,k}^{l} - \sum_{k \in K} EFN_{i,j-1,k}^{g} - \sum_{k \in K} EFN_{i,j-1,k}^{l} + \sum_{k \in K} ERP_{i-1,j,k}^{g}$$

$$+ \sum_{k \in K} ERP_{i-1,j,k}^{l} - \sum_{k \in K} ERN_{i-1,j,k}^{g} - \sum_{k \in K} ERN_{i-1,j,k}^{l} - \sum_{k \in K} EFP_{i,j,k}^{g} - \sum_{k \in K} EFP_{i,j,k}^{g}$$

$$+ \sum_{k \in K} EFN_{i,j,k}^{g} + \sum_{k \in K} EFN_{i,j,k}^{l} - \sum_{k \in K} ERP_{i,j,k}^{g} - \sum_{k \in K} ERP_{i,j,k}^{l} + \sum_{k \in K} ERN_{i,j,k}^{g}$$

$$+ \sum_{k \in K} ERN_{i,j,k}^{l} + \sum_{i',j' \in LN} \sum_{k \in K} EJ_{i',j',i,j,k}^{g} - \sum_{k \in K} EJ_{i',j',i,j,k}^{l} - \sum_{i',j' \in LN} \sum_{k \in K} EJ_{i,j,i',j',k}^{g}$$

$$- \sum_{i',j' \in LN} \sum_{k \in K} EJ_{i,j,i',j',k}^{l} + EM_{i,j} - EP_{i,j} + Q_{i,j}^{h} - Q_{i,j}^{c} + W_{i,j}^{com} - W_{i,j}^{exp} = 0, \quad \forall i, j$$

Here, where,  $Q_{i,j}^h \geq 0$  is the variable for the heat introduced into block  $B_{i,j}$  through hot utility streams,  $Q_{i,j}^c \geq 0$  is the variable for the heat withdrawn form block  $B_{i,j}$  via the cold utility streams,  $W_{i,j}^{com} \geq 0$  is the work energy added into block  $B_{i,j}$ , and  $W_{i,j}^{exp} \geq 0$  is the work energy removed from block  $B_{i,j}$ . Further details of the work calculations can be obtained from Demirel et al. (2017).<sup>49</sup> Individual stream enthalpy terms are defined as a function of flow rate, temperature and pressure. This functional relationship will depend on the phase, temperature and pressure of the source block. To determine the phase, we define the following binary variable:

$$z_{i,j}^{phase} = \begin{cases} 1 & \text{if } B_{i,j} \text{ is in vapor/gas phase} \\ 0 & \text{if } B_{i,j} \text{ is in liquid phase} \end{cases}$$

When  $z_{i,j}^{phase}$  is 1, block is in gas/vapor phase and when it is 0, block is in the liquid phase. Accordingly, enthalpy of a liquid stream in the horizontal forward direction can be described as follows:

$$EFP_{i,j,k}^{l} + EFP_{i,j,k}^{ls} = H^{liq}(FP_{i,j,k}, T_{i,j}, P_{i,j}) \quad \forall i, j, k$$
 (16)

$$EFP_{i,j,k}^{l} \le EU \times (1 - z_{i,j}^{phase}) \quad \forall i, j, k$$
 (17)

$$EFP_{i,j,k}^l \ge -EU \times (1 - z_{i,j}^{phase}) \quad \forall i, j, k$$
 (18)

$$EFP_{i,j,k}^{ls} \le EU \times z_{i,j}^{phase} \quad \forall i, j, k$$
 (19)

$$EFP_{i,j,k}^{ls} \ge -EU \times z_{i,j}^{phase} \quad \forall i, j, k$$
 (20)

Equation 16 assigns the liquid enthalpy of the horizontal flow in the positive direction to either  $EFP_{i,j,k}^l$  or  $EFP_{i,j,k}^{ls}$ .  $EFP_{i,j,k}^{ls}$  is a slack variable which is active when the source block is in vapor phase, i.e.  $z_{i,j}^{phase} = 1$ . In this case,  $EFP_{i,j,k}^l = 0$ . Similar logic applies for the vapor enthalpy terms and also for the remaining enthalpy terms which are provided in the Supporting Information.

**Phase Assignments**: Phase of a block is determined based on dew and bubble pressures as follows:

$$P_{i,j} \ge P_{i,j}^{bub}(P_{i,j}, T_{i,j}, y_{i,j,k}) - P_{i,j}^{bub,U} z_{i,j}^{phase} \quad \forall i, j \in LB$$
 (21)

$$P_{i,j} \le P_{i,j}^{dew}(P_{i,j}, T_{i,j}, y_{i,j,k}) + P_{i,j}^{max}(1 - z_{i,j}^{phase}) \quad \forall i, j \in VB$$
 (22)

Equation 21 states that the phase of a block will be liquid if the pressure of the block is greater than the bubble pressure of the mixture. Equation 22 states that the block is in vapor phase if the pressure of the block is lower than the dew pressure of the mixture. Bubble and dew pressures can be calculated based on different thermodynamic models and can be computationally demanding. To manage the problem complexity, we define LB and VB sets to denote the position of the blocks  $B_{i,j}$  at which the above constraints are utilized. If, however, these sets cover all the blocks within the superstructure, then the phase of each block can be automatically determined. If there is a product withdrawal from a block, then the block phase should satisfy the product phase requirements:

$$z_{i,j}^{phase} \ge z_{ps}^{phaseprod} - (1 - z_{i,j,ps}^{product}), \quad \forall i, j, ps$$
 (23)

$$z_{i,j}^{phase} \leq z_{ps}^{phaseprod} + (1 - z_{i,j,ps}^{product}), \quad \forall i, j, ps$$
 (24)

where  $z_{ps}^{phaseprod}$  is a 0-1 parameter defining the known phase of product stream ps. There can

be also additional phase constraints depending on the membrane types which are described in the corresponding section below.

**Block Boundary Assignments**: Each boundary between two neighboring blocks can be unrestricted, semi-restricted or completely restricted. We define the following binary variables to determine the boundary type:

$$z_{i,j}^{unF} = \begin{cases} 1 & \text{if boundary between } B_{i,j} \text{ and } B_{i,j+1} \text{ is unrestricted} \\ 0 & \text{otherwise} \end{cases}$$

$$z_{i,j}^{unR} = \begin{cases} 1 & \text{if boundary between } B_{i,j} \text{ and } B_{i+1,j} \text{ is unrestricted} \\ 0 & \text{otherwise} \end{cases}$$

$$z_{i,j}^{srF} = \begin{cases} 1 & \text{if boundary between } B_{i,j} \text{ and } B_{i,j+1} \text{ is semi-restricted} \\ 0 & \text{otherwise} \end{cases}$$

$$z_{i,j}^{srR} = \begin{cases} 1 & \text{if boundary between } B_{i,j} \text{ and } B_{i+1,j} \text{ is semi-restricted} \\ 0 & \text{otherwise} \end{cases}$$

$$z_{i,j}^{crF} = \begin{cases} 1 & \text{if boundary between } B_{i,j} \text{ and } B_{i,j+1} \text{ is completely restricted} \\ 0 & \text{otherwise} \end{cases}$$

$$z_{i,j}^{crR} = \begin{cases} 1 & \text{if boundary between } B_{i,j} \text{ and } B_{i+1,j} \text{ is completely restricted} \\ 0 & \text{otherwise} \end{cases}$$

For the boundary in the horizontal direction between block  $B_{i,j}$  and  $B_{i,j+1}$ , we define  $z_{i,j}^{unF}$ ,  $z_{i,j}^{srF}$  and  $z_{i,j}^{crF}$  to denote whether the boundary is unrestricted, semi-restricted and completely restricted, respectively. Similarly, in the vertical direction between block  $B_{i,j}$  and  $B_{i+1,j}$ , we define  $z_{i,j}^{unR}$ ,  $z_{i,j}^{srR}$  and  $z_{i,j}^{crR}$ . Only one of these boundary types can be selected for each boundary:

$$z_{i,j}^{unF} + z_{i,j}^{srF} + z_{i,j}^{crF} = 1, \quad \forall i, j$$
 (25)

$$z_{i,j}^{unR} + z_{i,j}^{srR} + z_{i,j}^{crR} = 1, \quad \forall i, j$$
 (26)

Unrestricted Boundary: An unrestricted flow is free of any mass transfer interception and the composition of each unrestricted stream should be the same with its source block.  $y_{i,j,k}$  denotes the molar composition of component k in block  $B_{i,j}$ . Accordingly, we write the following for each interblock stream:

$$FP_{i,j,k} \le y_{i,j,k} \sum_{k' \in K} FP_{i,j,k'} + FU\left(1 - z_{i,j}^{unF}\right), \quad \forall i, j, k$$

$$(27)$$

$$FP_{i,j,k} \ge y_{i,j,k} \sum_{k' \in K} FP_{i,j,k'} - FU\left(1 - z_{i,j}^{unF}\right), \quad \forall i, j, k$$
 (28)

$$FN_{i,j,k} \le y_{i,j+1,k} \sum_{k' \in K} FN_{i,j,k'} + FU\left(1 - z_{i,j}^{unF}\right), \quad \forall i, j, k$$
 (29)

$$FN_{i,j,k} \ge y_{i,j+1,k} \sum_{k' \in K} FN_{i,j,k'} - FU\left(1 - z_{i,j}^{unF}\right), \quad \forall i, j, k$$
 (30)

$$RP_{i,j,k} \le y_{i,j,k} \sum_{k' \in K} RP_{i,j,k'} + RU\left(1 - z_{i,j}^{unR}\right), \quad \forall i, j, k$$

$$(31)$$

$$RP_{i,j,k} \ge y_{i,j,k} \sum_{k' \in K} RP_{i,j,k'} - RU\left(1 - z_{i,j}^{unR}\right), \quad \forall i, j, k$$

$$(32)$$

$$RN_{i,j,k} \le y_{i+1,j,k} \sum_{k' \in K} RP_{i,j,k'} + RU\left(1 - z_{i,j}^{unR}\right), \quad \forall i, j, k$$

$$(33)$$

$$RN_{i,j,k} \ge y_{i+1,j,k} \sum_{k' \in K} RP_{i,j,k'} - RU\left(1 - z_{i,j}^{unR}\right), \quad \forall i, j, k$$
 (34)

where FU and RU represent the upper bound on the total flow rate allowed through a boundary.

**Product and Jump Flow Compositions**: All the jump and product streams leaving the block should also have the same composition with the other unrestricted outlet streams. Accordingly,

$$H_{i,j,k,ps} = y_{i,j,k} \sum_{k' \in K} H_{i,j,k',ps}, \quad \forall i, j, k, ps$$
(35)

$$J_{i,j,i',j',k} = y_{i,j,k} \sum_{k' \in K} J_{i,j,i',j',k'}, \quad \forall i, j, i', j' \in LN, \ \forall k$$
 (36)

Completely Restricted Boundary: Completely restricted boundary indicates a zero flow:

$$FL(1 - z_{i,j}^{crF}) \le F_{i,j,k} \le FU\left(1 - z_{i,j}^{crF}\right), \quad \forall i, j, k$$

$$(37)$$

$$RL(1 - z_{i,j}^{crR}) \le R_{i,j,k} \le RU\left(1 - z_{i,j}^{crR}\right), \quad \forall i, j, k$$
(38)

Semi-restricted Boundary: Semi-restricted boundary might represent a direct phase contact between two distinct phases or it can stand for a membrane material. In this work, we consider only the membrane type boundaries. For other types, please see the previous works. <sup>49,50</sup> We define  $z_{i,j,s,m}^F$  as the variable to indicate which separation phenomenon and enabling material is activated for horizontal semi-restricted boundary. When  $z_{i,j,s,m}^F$  is one, there exists a semi-restricted boundary between block  $B_{i,j}$  and  $B_{i,j+1}$  with separation phenomenon s and enabling material m.

$$z_{i,j,s,m}^F = \begin{cases} 1 & \text{if the boundary between } B_{i,j} \text{ and } B_{i,j+1} \text{ is occupied by} \\ & \text{phenomena } s \text{ with material } m \\ 0 & \text{otherwise} \end{cases}$$

Similarly in the vertical direction:

$$z_{i,j,s,m}^{R} = \begin{cases} 1 & \text{if the boundary between } B_{i,j} \text{ and } B_{i+1,j} \text{ is occupied by} \\ & \text{phenomena } s \text{ with material } m \\ 0 & \text{otherwise} \end{cases}$$

A semi-restricted boundary can be assigned with only one permeation phenomenon and only one corresponding membrane material:

$$z_{i,j}^{srF} = \sum_{(s,m)\in SM} z_{i,j,s,m}^F, \quad \forall i, j$$
 (39)

$$z_{i,j}^{srR} = \sum_{(s,m)\in SM} z_{i,j,s,m}^R, \quad \forall i, j$$
 (40)

SM describes the membrane materials m available for permeation phenomenon s.

Modeling Membrane Boundaries: When a boundary is assigned with a membrane material, mass transfer rate through it is calculated by using the corresponding flux model as a function of the chemical potential gradient across the membrane, mass transfer coefficients of the individual components and the size of the membrane boundary. Accordingly, we define  $\mu_{i,j,k,s,m}$  as the chemical potential at block  $B_{i,j}$  with a membrane boundary m associated with phenomenon s for each component k. Mass transfer coefficient of component k through the semi-restricted boundary with phenomenon s and material m is defined as  $\lambda_{i,j,k,s,m}$ . Membrane boundary areas are defined as  $A_{i,j,s,m}^F$  and  $A_{i,j,s,m}^F$  for the horizontal and vertical boundaries, respectively.

Mass transfer coefficients can be described as a function of the sorption and diffusion coefficients and membrane thickness or taken as a lumped parameter as permeance:

$$\lambda_{i,j,k,s,m} = f^{mt}(y_{i,j,k}, T_{i,j}, P_{i,j}, \beta_{k,s,m}), \quad \forall i, j, k, \ (s,m) \in SM$$
 (41)

while  $\beta_{k,s,m}$  describes a vector of membrane and component specific parameters including diffusion coefficients and material thickness.  $\lambda_{i,j,k,s,m}$  can be also taken as constant by assuming negligible change with composition, temperature and pressure. Furthermore, it can be taken as a variable and the overall performance of the membrane-based operation can be studied for revealing optimal membrane material properties. Membrane boundary areas can be also written as a function of the membrane dimensions, e.g. thickness, length, number of fibers, and can be subject to a set of equality and inequality constraints.

Based on these definitions, flow rate through a membrane boundary can be written as follows in the horizontal direction:

$$F_{i,j,k} \ge \lambda_{i,j,k,s,m} \times (\mu_{i,j,k,s,m} - \mu_{i,j+1,k,s,m}) \times A_{i,j,s,m}^{F} - M_{i,j,k,s,m}^{rateF} \times (1 - z_{i,j,s,m}^{F}), \quad \forall i, j, k, \ (s,m) \in SM$$
(42)

$$F_{i,j,k} \leq \lambda_{i,j,k,s,m} \times (\mu_{i,j,k,s,m} - \mu_{i,j+1,k,s,m}) \times A_{i,j,s,m}^{F} + M_{i,j,k,s,m}^{rateF} \times (1 - z_{i,j,s,m}^{F}), \quad \forall i, j, k, \ (s,m) \in SM$$
(43)

Here,  $F_{i,j,k}$  is a free variable for which the sign is determined by the chemical potential difference. If it is negative (positive), then the flow direction will be in the negative (positive) direction. Similar constraints can be also written in the vertical direction:

$$R_{i,j,k} \ge \lambda_{i,j,k,s,m} \times (\mu_{i,j,k,s,m} - \mu_{i+1,j,k,s,m}) \times A_{i,j,s,m}^{R} - M_{i,j,k,s,m}^{rateR} \times (1 - z_{i,j,s,m}^{R}), \quad \forall i, j, k, \ (s,m) \in SM$$
(44)

$$R_{i,j,k} \le \lambda_{i,j,k,s,m} \times (\mu_{i,j,k,s,m} - \mu_{i+1,j,k,s,m}) \times A_{i,j,s,m}^{R} + M_{i,j,k,s,m}^{rateR} \times (1 - z_{i,j,s,m}^{R}), \quad \forall i, j, k, \ (s,m) \in SM$$
(45)

The gradient across the membrane can be related to concentration, pressure, temperature and electromotive force and its permeate and retentate counterparts can be different based on the phases of the each and the related assumptions involved in describing the chemical potential. Accordingly, we can rewrite the above mass transfer rate constraints by defining separate chemical potential terms for the permeate and retentate sides:  $\mu_{i,j,k,s,m}^{per}$  and  $\mu_{i,j,k,s,m}^{ret}$ . Then, depending on the phenomenon and membrane material assigned to the semi-restricted boundary and whether the block acts as a permeate or retentate side, flow rate through a membrane boundary can be described based on the logical relations below. In the horizontal direction, if the block on the left is assigned as the retentate and the block on the right is assigned as the permeate side, these constrains become:

$$FP_{i,j,k} \ge \lambda_{i,j,k,s,m} \times \left(\mu_{i,j,k,s,m}^{ret} - \mu_{i,j+1,k,s,m}^{per}\right) \times A_{i,j,s,m}^{F}$$

$$- M_{i,j,k,s,m}^{rateF} \times \left(2 - z_{i,j,s,m}^{F} - z_{i,j}^{Fplus}\right), \quad \forall i, j, k, \ (s,m) \in SM$$

$$(46)$$

$$FP_{i,j,k} \leq \lambda_{i,j,k,s,m} \times \left(\mu_{i,j,k,s,m}^{ret} - \mu_{i,j+1,k,s,m}^{per}\right) \times A_{i,j,s,m}^{F}$$

$$+ M_{i,j,k,s,m}^{rateF} \times \left(2 - z_{i,j,s,m}^{F} - z_{i,j}^{Fplus}\right), \quad \forall i, j, k, \ (s,m) \in SM$$

$$(47)$$

If, on the other hand, block on the left is assigned as the permeate and block on the right is

assigned as the retentate side, these constrains become:

$$FN_{i,j,k} \ge \lambda_{i,j,k,s,m} \times \left(\mu_{i,j+1,k,s,m}^{ret} - \mu_{i,j,k,s,m}^{per}\right) \times A_{i,j,s,m}^{F}$$

$$- M_{i,j,k,s,m}^{rateF} \times \left(1 - z_{i,j,s,m}^{F} + z_{i,j}^{Fplus}\right), \quad \forall i, j, k, \ (s,m) \in SM$$

$$(48)$$

$$FN_{i,j,k} \leq \lambda_{i,j,k,s,m} \times \left(\mu_{i,j+1,k,s,m}^{ret} - \mu_{i,j,k,s,m}^{per}\right) \times A_{i,j,s,m}^{F} + M_{i,j,k,s,m}^{rateF} \times \left(1 - z_{i,j,s,m}^{F} + z_{i,j}^{Fplus}\right), \quad \forall i, j, k, \ (s,m) \in SM$$
(49)

Similar constraints can be also written in the vertical direction:

$$RP_{i,j,k} \ge \lambda_{i,j,k,s,m} \times \left(\mu_{i,j,k,s,m}^{ret} - \mu_{i+1,j,k,s,m}^{per}\right) \times A_{i,j,s,m}^{R} - M_{i,j,k,s,m}^{rateR} \times \left(2 - z_{i,j,s,m}^{R} - z_{i,j}^{Rplus}\right), \quad \forall i, j, k, \ (s,m) \in SM$$
(50)

$$RP_{i,j,k} \leq \lambda_{i,j,k,s,m} \times \left(\mu_{i,j,k,s,m}^{ret} - \mu_{i+1,j,k,s,m}^{per}\right) \times A_{i,j,s,m}^{R} + M_{i,j,k,s,m}^{rateR} \times \left(2 - z_{i,j,s,m}^{R} - z_{i,j}^{Rplus}\right), \quad \forall i, j, k, \ (s,m) \in SM$$
(51)

$$RN_{i,j,k} \ge \lambda_{i,j,k,s,m} \times \left(\mu_{i+1,j,k,s,m}^{ret} - \mu_{i,j,k,s,m}^{per}\right) \times A_{i,j,s,m}^{R} - M_{i,j,k,s,m}^{rateR} \times \left(1 - z_{i,j,s,m}^{R} + z_{i,j}^{Rplus}\right), \quad \forall i, j, k, \ (s,m) \in SM$$
(52)

$$RN_{i,j,k} \leq \lambda_{i,j,k,s,m} \times \left(\mu_{i+1,j,k,s,m}^{ret} - \mu_{i,j,k,s,m}^{per}\right) \times A_{i,j,s,m}^{R}$$

$$+ M_{i,j,k,s,m}^{rateR} \times \left(1 - z_{i,j,s,m}^{R} + z_{i,j}^{Rplus}\right), \quad \forall i, j, k, \ (s,m) \in SM$$

$$(53)$$

Description of the chemical potential terms in the above constraints differ according to the permeation phenomena and mixing assumptions. Accordingly, different models can be formulated. We first list here descriptions according to the different permeation phenomenon with complete mixing assumption. If one assumes complete mixing at both permeate and retentate sides, then the block (molar) composition variable  $y_{i,j,k}$  is used in describing these driving force terms. For gas permeation  $(GP \in S)$  and vapor permeation  $(VP \in S)$ , for instance, permeate and retentate driving force terms become the following with the ideal gas assumption:

$$\mu_{i,j,k,s,m}^{per} = P_{i,j} \times y_{i,j,k}, \ \forall i, j, k, (s,m) \in SM, s \in \{GP, VP\}$$
 (54)

$$\mu_{i,j,k,s,m}^{ret} = P_{i,j} \times y_{i,j,k}, \ \forall i, j, k, (s,m) \in SM, s \in \{GP, VP\}$$
 (55)

For the pervaporation, the same relationship is generally used for the permeate side. However, the retentate side driving force term is written based on the liquid activity coefficients as follows:

$$\mu_{i,j,k,s,m}^{ret} = P_{i,j,k}^{sat} \times y_{i,j,k} \times \gamma_{i,j,k,s,m}, \ \forall i, j, k, (s, m) \in SM, s \in \{PV\}$$
 (56)

where vapor pressures and activity coefficients are written as follows:

$$P_{i,j,k}^{sat} = \exp\left(A_k - \frac{B_k}{C_k + T_{i,j}}\right) \quad , \quad \forall i, j, \ k \in KH$$
 (57)

$$\gamma_{i,j,k,s,m} = f^{ther} \left( y_{i,j,k}, P_{i,j}, T_{i,j}, a_{k,s,m}^{th} \right), \quad \forall i, j, \ k \in K^{th}, (s, m) \in SM, s \in \{PV\}$$
(58)

where  $A_k$ ,  $B_k$  and  $C_k$  are the Antoine parameters for component k. KH designates the components for which the given Antoine equation holds for vapor pressure calculation. Equation 58 stands for a set of equality constraints describing the liquid activity coefficients  $\gamma_{i,j,k,s,m}$  as a function of block variables and a set of thermodynamic model parameters, i.e.  $a_{k,s,m}^{th}$ , which can be described with different thermodynamic models for different membrane material m with permeation phenomenon s.  $K^{th}$  includes the chemical components k that follow the given liquid activity coefficient model.

We need to also ensure several phase constraints for each membrane type. For instance, if the boundary is assigned with a gas/vapor separation membrane, then the two blocks separated by the membrane should be in the gas phase. This leads to the following constraints:

$$z_{i,j}^{phase} \ge z_{i,j,s,m}^{F} \quad \forall i, j, (s,m) \in SM, s \in \{GP, VP\}$$
 (59)

$$z_{i,j+1}^{phase} \ge z_{i,j,s,m}^{F} \quad \forall i, j, (s,m) \in SM, s \in \{GP, VP\}$$
 (60)

$$z_{i,j}^{phase} \ge z_{i,j,s,m}^{R} \quad \forall i, j, (s,m) \in SM, s \in \{GP, VP\}$$
 (61)

$$z_{i+1,j}^{phase} \ge z_{i,j,s,m}^R \quad \forall i, j, (s,m) \in SM, s \in \{GP, VP\}$$

$$\tag{62}$$

Equations 59-60 states that if a horizontal boundary is assigned with a membrane material associated with gas or vapor permeation, then the phase of the two neighboring blocks should be in gas phase. Otherwise, these phase relations become redundant. Equations 61-62 states the same in the vertical direction. For some other membrane types, the two sides of the membrane might be needed to be in different phases, e.g. membrane absorption, stripping, pervaporation. For pervaporation, for instance, while the retentate side is in liquid phase, permeate side is in vapor phase. In the horizontal direction, this can be ensured via the following constraints:

$$z_{i,j}^{phase} \le 2 - z_{i,j,s,m}^{F} - z_{i,j}^{Fplus}, \quad \forall i, j, (s, m) \in SM, s \in \{PV\}$$
 (63)

$$z_{i,j+1}^{phase} \ge -1 + z_{i,j,s,m}^{F} + z_{i,j}^{Fplus}, \quad \forall i, j, (s,m) \in SM, s \in \{PV\}$$
 (64)

$$z_{i,j+1}^{phase} \le 1 - z_{i,j,s,m}^{F} + z_{i,j}^{Fplus}, \quad \forall i, j, (s, m) \in SM, s \in \{PV\}$$
 (65)

$$z_{i,j}^{phase} \ge z_{i,j,s,m}^{F} - z_{i,j}^{Fplus}, \quad \forall i, j, (s, m) \in SM, s \in \{PV\}$$
 (66)

If the horizontal boundary is assigned with a pervaporation membrane material, i.e.  $z_{i,j,s,m}^F = 1$ , and the block on the left is assigned as retentate side, i.e. flow is towards from the block on the left to the right and  $z_{i,j}^{Fplus} = 1$ , then Eqs. 63-64 become active and  $z_{i,j}^{phase} = 0$  and  $z_{i,j+1}^{phase} = 1$ . Equations 65-66 ensures the same when the block on the left is assigned as the permeate side. Similar constraints can be also written in the vertical direction.

Different Modeling Approaches: The above relations on the driving force assumes complete mixing through a single block. There can be also other short-cut membrane models. One can simply take the retentate feed composition for the retentate driving force calculation. Also, retentate side concentration can be approximated as the logarithmic average between the feed and outlet compositions. These type of mixing models require calculation of inlet

#### block compositions:

$$\Phi_{i,j,k} = FP_{i,j-1,k} + FN_{i,j,k} + RP_{i-1,j,k} + RN_{i,j,k} + \sum_{fs} M_{i,j,k,fs}^{feed} + \sum_{i',j' \in LN} J_{i,j,i',j',k}, \quad \forall i, j, k \quad (67)$$

$$\Phi_{i,j,k} = y_{i,j,k}^{in} \sum_{k'} \Phi_{i,j,k'}, \quad \forall i, j, k$$

$$(68)$$

Here,  $\Phi_{i,j,k}$  denotes the total inlet flow rate into the block  $B_{i,j}$  and it is comprised of interblock streams, jump inlet streams and external feed streams.  $y_{i,j,k}^{in}$  denotes the inlet composition for block  $B_{i,j}$ . Accordingly, if one assumes that the driving force for the retentate side is a function of the inlet composition, then, for pervaporation membranes for example, Eq. 56 can be modified as follows:

$$\mu_{i,j,k,s,m}^{ret} = P_{i,j,k}^{sat} \times y_{i,j,k}^{in} \times \gamma_{i,j,k,s,m}, \ \forall i, j, k, (s,m) \in SM, s \in \{PV\}$$
 (69)

If one uses a logarithmic mean between inlet and outlet concentrations for the retentate side, then the driving force term, for vapor/gas permeations, for instance, can be written as below:

$$y_{i,j,k}^{log} = \frac{y_{i,j,k}^{in} - y_{i,j,k}}{\ln\left(\frac{y_{i,j,k}^{in}}{y_{i,j,k}}\right)}, \quad \forall i, j, k$$
 (70)

$$\mu_{i,j,k,s,m}^{ret} = P_{i,j} \times y_{i,j,k}^{log}, \ \forall i, j, k, (s,m) \in SM, s \in \{GP, VP\}$$
 (71)

To avoid numerical problems, Eq. 70 can be reformulated with Chen's approximation:

$$y_{i,j,k}^{log} = \left[ y_{i,j,k} \times y_{i,j,k}^{in} \times \left( \frac{y_{i,j,k} + y_{i,j,k}^{in}}{2} \right) \right]^{1/3}, \quad \forall i, j, k$$
 (72)

Note that these driving force terms are utilized in short-cut models when the whole membrane module is represented by a single semi-restricted boundary as shown in Figure 1c-ii.

Maximum Stage-cut Constraints: One issue with the presented model is that if there is no nonzero unrestricted interblock streams, product streams or outgoing jump

streams, the block outlet concentrations can be arbitrarily chosen. In this case, as the block composition variables becomes arbitrary, membrane boundaries can act as ideal separators rather than following the given driving force constraints. This is particularly problematic if one allows a block to be assigned with multiple membrane boundaries and includes membranes with concentric layers in the solution space (as shown in Figure 2f). As a remedy, we need to ensure that there exists at least one non-zero flow exiting a block with the interblock, product or jump streams (retentate) apart from the ones associated with the semi-restricted boundaries (permeate). This is indeed closely related to a membrane separation efficiency parameter named stage cut. Stage cut is defined as the ratio of the permeate flow to the feed flow. Hence, this requirement is similar to providing an upper bound on the maximum stage cut that can be achieved through a membrane boundary. This ensures that there exists at least one non-zero retentate flow and block compositions are accurately calculated. Accordingly, we define  $\theta^{max} < 1$  as the parameter designating the maximum stage-cut for the membrane boundaries and write the following constraints:

$$(1 - \theta^{max}) \sum_{k} \Phi_{i,j,k} \leq FP_{i,j}^{un} + RP_{i,j}^{un} + FN_{i,j-1}^{un} + RN_{i-1,j}^{un} + \sum_{k,ps} H_{i,j,k,ps} + \sum_{i',j' \in LN,k \in K} J_{i,j,i',j',k}, \ \forall i,j$$

$$(73)$$

$$FP_{i,j}^{un} \leq FUz_{i,j}^{unF}; \quad FP_{i,j}^{un} \geq \sum_{k} FP_{i,j,k} - FU\left(1 - z_{i,j}^{unF}\right); \quad FP_{i,j}^{un} \leq \sum_{k} FP_{i,j,k}, \ \forall i,j \ (74)$$

$$FN_{i,j}^{un} \leq FUz_{i,j}^{unF}; \quad FN_{i,j}^{un} \geq \sum_{k} FN_{i,j,k} - FU\left(1 - z_{i,j}^{unF}\right); \quad FN_{i,j}^{un} \leq \sum_{k} FN_{i,j,k}, \ \forall i,j \ (75)$$

$$RP_{i,j}^{un} \leq RUz_{i,j}^{unR}; \quad RP_{i,j}^{un} \geq \sum_{k} RP_{i,j,k} - RU\left(1 - z_{i,j}^{unR}\right); \quad RP_{i,j}^{un} \leq \sum_{k} RP_{i,j,k} \ \forall i,j \ (76)$$

$$RN_{i,j}^{un} \le RUz_{i,j}^{unR}; \quad RN_{i,j}^{un} \ge \sum_{k} RN_{i,j,k} - RU\left(1 - z_{i,j}^{unR}\right); \quad RP_{i,j}^{un} \le \sum_{k} RP_{i,j,k} \quad \forall i, j \quad (77)$$

Equation 73 states that the certain fraction of the total inlet flow into a block, determined by  $\theta^{max}$ , should exit the block through either unrestricted interblock streams, product streams and/or jump streams. Here,  $FP_{i,j}^{un}$ ,  $FN_{i,j}^{un}$ ,  $RP_{i,j}^{un}$  and  $RN_{i,j}^{un}$  are equal to the total flow rates of the corresponding interblock streams, i.e.  $FP_{i,j,k}$ ,  $FN_{i,j,k}$ ,  $RP_{i,j,k}$  and  $RN_{i,j,k}$ , respectively,

if their boundaries are selected as unrestricted. For instance, if a stream flowing in horizontal forward direction,  $FP_{i,j,k}$ , is going through an unrestricted boundary, i.e.  $z_{i,j}^{unF} = 1$ , then  $FP_{i,j}^{un}$  becomes equal to the total flow through this boundary, i.e.  $\sum_k FP_{i,j,k}$ . Otherwise, it becomes zero. This is satisfied through Eqs. 74. Similar relations are also written for the other interblock streams with Eqs. 75-77.

### 3.3 Objective Functions and Multi-objective Optimization

Different objective functions can be used when utilizing the building block-based approach for membrane-based process synthesis. Here, we list several examples of these objective functions along with a multi-objective problem formulation.

**Maximization of Product Recovery**: A desired product stream  $\tilde{p}$  with a certain purity specification for component  $\tilde{k}$  as  $y_{k=\tilde{k},ps=\tilde{p}}^{MIN,prod}$  can be maximized as follows:

$$\max \sum_{i \in I} \sum_{j \in J} \sum_{k \in K} H_{i,j,k,ps=\tilde{p}} \tag{78}$$

**Maximization of Product Purity**: Purity of a component  $\tilde{k}$  in a desired product stream with minimum recovery of  $D_{ps=\tilde{p}}^{min}$ , can be maximized using the following objective function:

$$\max \frac{\sum_{i \in I} \sum_{j \in J} H_{i,j,k=\tilde{k},ps=\tilde{p}}}{\sum_{i \in I} \sum_{j \in J} \sum_{k \in K} H_{i,j,k,ps=\tilde{p}}}$$

$$(79)$$

Minimization of Energy Consumption: Total energy consumption of the membrane-based process can be minimized with the following objective function:

$$\min \ \omega_1 \ \sum_{i \in I} \sum_{j \in J} \left( Q_{i,j}^h + Q_{i,j}^c \right) + \ \omega_2 \sum_{i \in I} \sum_{j \in J} \frac{1}{\eta_c} (W_{i,j}^{com})$$
 (80)

Here,  $\eta_c$  is the compressor efficiency, and  $\omega_1$  and  $\omega_2$  are parameters used to designate different weights on heat and work energy. Either one of them can be taken as zero to consider the minimization of only one form of energy. Or they can be used to convert one form to the other and perform overall energy minimization.

*Minimization of Operating Costs*: The operating cost includes the costs of heating, cooling, raw materials, and compression:

min 
$$UC_{hu} \sum_{i \in I} \sum_{j \in J} Q_{i,j}^{h} + UC_{cu} \sum_{i \in I} \sum_{j \in J} Q_{i,j}^{c} + \sum_{i \in I} \sum_{j \in J} \sum_{k \in K} \sum_{fs \in FS} UC_{fs} M_{i,j,k,fs}^{feed}$$

$$+ \frac{UC_{elect}}{\eta_{c}} \sum_{i \in I} \sum_{j \in J} W_{i,j}^{com} + UC_{rep} \left( a^{m} \sum_{i,j,(s,m) \in SM} \left[ A_{i,j,s,m}^{F} \right]^{b_{m}} + a^{m} \sum_{i,j,(s,m) \in SM} \left[ A_{i,j,s,m}^{R} \right]^{b_{m}} \right)$$
(81)

where,  $UC_{hu}$ ,  $UC_{cu}$ ,  $UC_{fs}$  and  $UC_{elect}$  represent the unit cost of hot utility, cold utility, feed and electricity, respectively.  $UC_{rep}$  (year<sup>-1</sup>) is the parameter denoting replacement frequency of the membrane modules. Replacement cost is calculated as a function of the capital cost of the membrane modules.

*Minimization of Total Annualized Cost*: The total annualized cost (TAC) of the membrane-based process including operating and capital costs can be formulated as follows:

$$\min \ UC_{hu} \sum_{i \in I} \sum_{j \in J} Q_{i,j}^{h} + UC_{cu} \sum_{i \in I} \sum_{j \in J} Q_{i,j}^{c} + \sum_{i \in I} \sum_{j \in J} \sum_{k \in K} \sum_{f \in FS} UC_{fs} M_{i,j,k,fs}^{feed} \\
+ \frac{UC_{elect}}{\eta_{c}} \sum_{i \in I} \sum_{j \in J} W_{i,j}^{com} \\
+ UC_{rep} \left( a^{m} \sum_{i,j,(s,m) \in SM} \left[ A_{i,j,s,m}^{F} \right]^{b_{m}} + a^{m} \sum_{i,j,(s,m) \in SM} \left[ A_{i,j,s,m}^{R} \right]^{b_{m}} \right) \\
+ \alpha^{TAC} \left[ a^{heat} \sum_{i,j} \left[ \frac{Q_{i,j}^{h}}{U^{h}LMTD_{i,j}^{h}} \right]^{b_{h}} + a^{cool} \sum_{i,j} \left[ \frac{Q_{i,j}^{c}}{U^{c}LMTD_{i,j}^{c}} \right]^{b_{c}} + a^{com} \sum_{i,j} \left[ W_{i,j}^{com} \right]^{b_{com}} \right. \\
+ a^{m} \sum_{i,j,(s,m) \in SM} \left[ A_{i,j,s,m}^{F} \right]^{b_{m}} + a^{m} \sum_{i,j,(s,m) \in SM} \left[ A_{i,j,s,m}^{R} \right]^{b_{m}} \\
+ a^{mf} \sum_{i,j,(s,m) \in SM} \left[ z_{i,j,s,m}^{F} + z_{i,j,s,m}^{R} \right] \right]$$
(82)

The first five terms are related with the operational costs similar to Eq. 81. The rest of the objective function denotes the capital costs and  $\alpha^{TAC}$  denotes the capital recovery factor. The sixth and seventh terms are for the heater and cooler capital cost calculations. The eighth

term is for the compressor capital costs. The ninth and tenth terms are for the membrane capital costs for the horizontal and vertical boundaries, respectively. The last term denotes the fixed capital costs due to the membrane operation if there is any.

Multi-objective Optimization: There exists several trade-offs between the aforementioned objectives. These trade-offs include the ones between energy consumption and membrane areas, i.e. capital costs, and purity and recovery. We use  $\epsilon$ -constraint method to reveal the extent of these trade-offs. We choose one of the objectives as the primary objective and keep the others as the inequality constraints in the optimization formulation. With a successive change of the bounds on these constraints, solutions of the optimization problems reveal a set of different membrane-processes and a pareto space demonstrating the nature of these trade-offs. Below, we provide an example on multi-objective problem formulation for maximization of product purity for a component  $\tilde{k}$  in a product stream  $\tilde{p}$  while also maximizing the recovery of the product stream  $\tilde{p}$ :

$$\max \sum_{i \in I} \sum_{j \in J} \sum_{k \in K} H_{i,j,k,ps=\tilde{p}}$$

$$s.t. \quad \frac{H_{i,j,k=\tilde{k},ps=\tilde{p}}}{\sum_{k' \in K} H_{i,j,k',ps=\tilde{p}}} \ge \epsilon \quad \forall i, j$$
(83)

We pose the product recovery maximization as the primary objective which is the same as Eq. 78. The purity objective is met via  $\epsilon$  constraint. The parameter  $\epsilon$  stands for the minimum purity of  $\tilde{k}$  in product stream  $\tilde{p}$ . By solving the problem for different values of  $\epsilon$ , we obtain a Pareto front that reveals the trade-offs between the product recovery and the product purity, while synthesizing optimal membrane process configurations. An example of such multi-objective optimization is provided in the next section. Objectives other than purity and recovery can be also treated in similar fashion.

### 4 Case Studies

The building block representation and its associated MINLP model can be utilized for several

purposes in several ways. First, one can automatically generate different membrane processes by treating the boundary types, directions and the flow rates of the active streams as degrees of freedom. Case study 1 is an example of this, where optimal flowsheet variants are generated for a specific design problem related to methane/nitrogen separation. The applicability of the multi-objective optimization formulation is also demonstrated through this example. Second, one can also optimize and further study only a limited number of promising design alternatives by simply fixing the positions of the membrane modules in the superstructure. We illustrate this through Case Study 2 concerning a vapor permeation membrane-based methanol/water separation. Third, the building block representation leads to a generic superstructure-based process synthesis framework to find most cost-effective membrane networks with optimal module configurations, flow patterns and recycle options. This is demonstrated in Case Study 3 that focuses on the synthesis of a gas separation membrane network. While addressing the case studies, we assumed isothermal membrane operation and neglected gas/vapor throttling and concentration polarization.

#### 4.1 Automated Generation of Membrane-based Processes

In this case study, we show how building block-based approach can be used to automatically generate different membrane-based processes with a literature problem on CH<sub>4</sub>-N<sub>2</sub> separation taken from Mohammadi et al. (2020).<sup>46</sup> In U.S., around 16% of the currently known gas reserves contain N<sub>2</sub> which must be separated for fuel or pipeline grade CH<sub>4</sub>.<sup>55</sup> Membrane-based processes can be used as modular units to achieve high purity methane. Accordingly, the objective is to develop an optimal membrane separation system for purifying a feed stream with 10 MMscfd containing 90 % CH<sub>4</sub> and 10 %N<sub>2</sub> (mole percent) at 500 psia. There is an inherent trade-off between the recovery and the purity. To investigate these trade-offs, we use multi-objective optimization to generate optimal processes with maximum CH<sub>4</sub> recovery and purity. We consider a N<sub>2</sub> selective membrane with 50 GPU (Gas Permeation Unit) permeance toward N<sub>2</sub> and 20 GPU toward CH<sub>4</sub>.<sup>56</sup> Similar to the

reference work, we consider that the pressure of permeate and retentate sides are operated at 100 and 500 psia, respectively, at 30°C. Higher separation performance can be achieved with higher membrane areas. Hence, the upper bound on membrane modules are crucial in revealing the maximum purity and recovery of the membrane process. We assume a 25000 m<sup>2</sup> of area per membrane module as the upper bound. Although the reference work did not specify any bound for the N<sub>2</sub> selective membranes, they report membrane areas of greater than 190000 m<sup>2</sup> for the CH<sub>4</sub> selective membrane processes. Our results show that more cost-effective and better solutions are possible which also require much smaller membrane areas (25000 m<sup>2</sup> or less).

To describe the flux through membrane, we use logarithmic mean of the feed and outlet concentrations at the retentate side and assume complete mixing at the permeate as is the case in the reference work. This indicates that two neighboring building blocks sharing a common semi-restricted membrane boundary is sufficient to represent a membrane module. Before addressing the problem with building block superstructure with multi-objective optimization, we first show that the same solutions as in the reference work can be obtained through the building block superstructure while using a single objective, i.e. maximization of the product recovery.

For a separation system with two membrane modules for 95% CH<sub>4</sub> purity in the product, Mohammadi et al. (2020) reports the solution given in Figure 4a as the optimal solution which yields 71.36% CH<sub>4</sub> recovery. This process can be represented by using building superstructure as shown in Figure 4a. The first row of the blocks represents the retentate side, the second row represents the permeate side. The recycle streams and the connections from the first membrane permeate to the second membrane retentate are represented through the jump streams. This gives the same process topology with the same connections. To replicate the previously reported solution, we simply fix several variables to the values reported in the literature. Specifically, we specify the membrane areas for the semi-restricted boundaries and fix the retentate composition for the second membrane. This reduces the degrees-of-freedom.

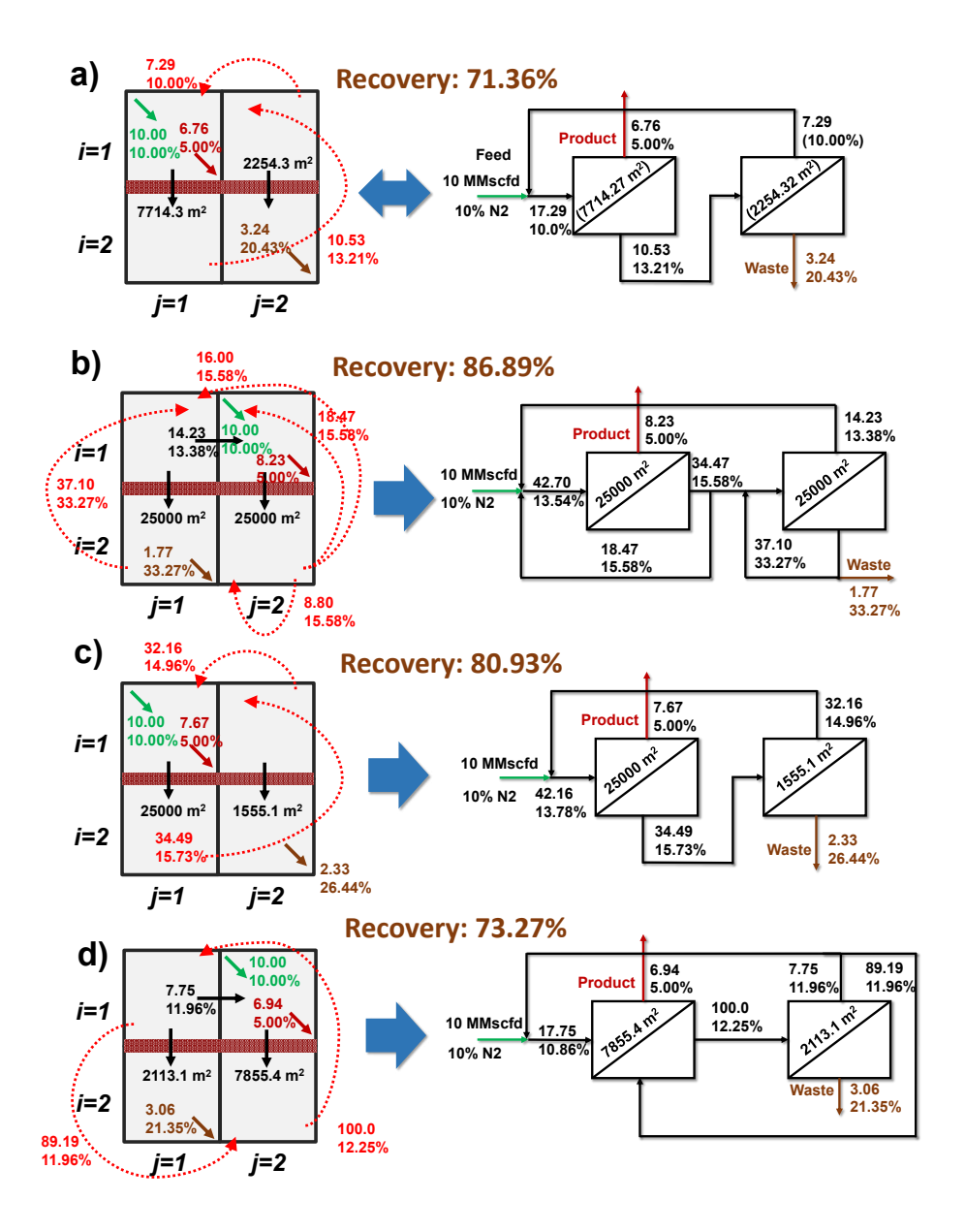


Figure 4: Optimal membrane networks generated with building block superstructure for CH<sub>4</sub> recovery from natural gas with 95% purity. a) The optimal result reported by Mohammadi et al. (2020)<sup>46</sup> (right) and its building block solution (left). Numbers in paranthesis denote the variables fixed to obtain the same solution with building blocks. b) Result generated with building block superstructure without any structural specification (left) and the corresponding membrane network (right). c) Optimal building block result (left) and the corresponding membrane network (right) when only the same connections with the reference are allowed. d) Optimal building block result (left) and the corresponding membrane network (right) when the upper bound on the total membrane area is restricted to the optimal reference solution.

# Solving this problem yields 71.36% CH<sub>4</sub> recovery, which is the same as the solution reported previously.

After verifying that the reported solution is embedded within the building superstructure, we solve the same problem without any prior specification of the boundary types, membrane areas, jump streams or any block composition with  $2\times 2$  superstructure. This allows any boundary within this  $2\times 2$  superstructure to be assigned with the membrane material, any block to accept the fresh feed stream and reject either waste or product streams. We allow only one semi-restricted for a block which restricts the total number of membrane modules to 2. This can be either in vertical or horizontal direction. Hence, we allow only the vertical boundaries to be assigned with the membrane material. This reduces the symmetry within the superstructure. Problem contains 189 variables (10 binary variables), 251 constraints, 925 non-zero elements. We solve this problem with BARON for 90 mins with maximization CH<sub>4</sub> recovery as the objective. While upper bound is obtained within seconds, we solve the problem further to see whether any improvement in the lower bound is possible. The lower bound does not improve and the reported solution is within 14% of the optimality gap. The optimal membrane process is shown in Figure 4b along with the building block solution. This process results in more than 86% CH<sub>4</sub> recovery while delivering the same purity level as the reference flowsheet. Yet, this process enables 22% increase in the overall CH<sub>4</sub> recovery. Although the retentate-retentate recycle stream is still utilized, building block result suggests three new recycle streams. Two of these recycle streams require the permeate outlet streams to be fed back to the retentate sides of the same modules. The third new recycle stream is from the permeate outlet of the first module to the permeate inlet of the same module. As there is complete mixing in the permeate sides, this permeate-permeate recycle stream is actually redundant and can be eliminated. Hence, this is not shown on the equivalent flowsheet representation.

To demonstrate the other possible membrane systems that are included in the solution space, we also solve the same problem by only allowing the same connections with the base-case design. When this problem is solved, the membrane process as shown in Figure 4c is obtained. The recovery is about 81% which is 13% higher than the base-case. This process still yields higher product recovery than the reference, although delivering less recovery than the best optimal building block process shown in Figure 4b. This also shows the benefit of the recycle streams identified by the building block superstructure in that process. One

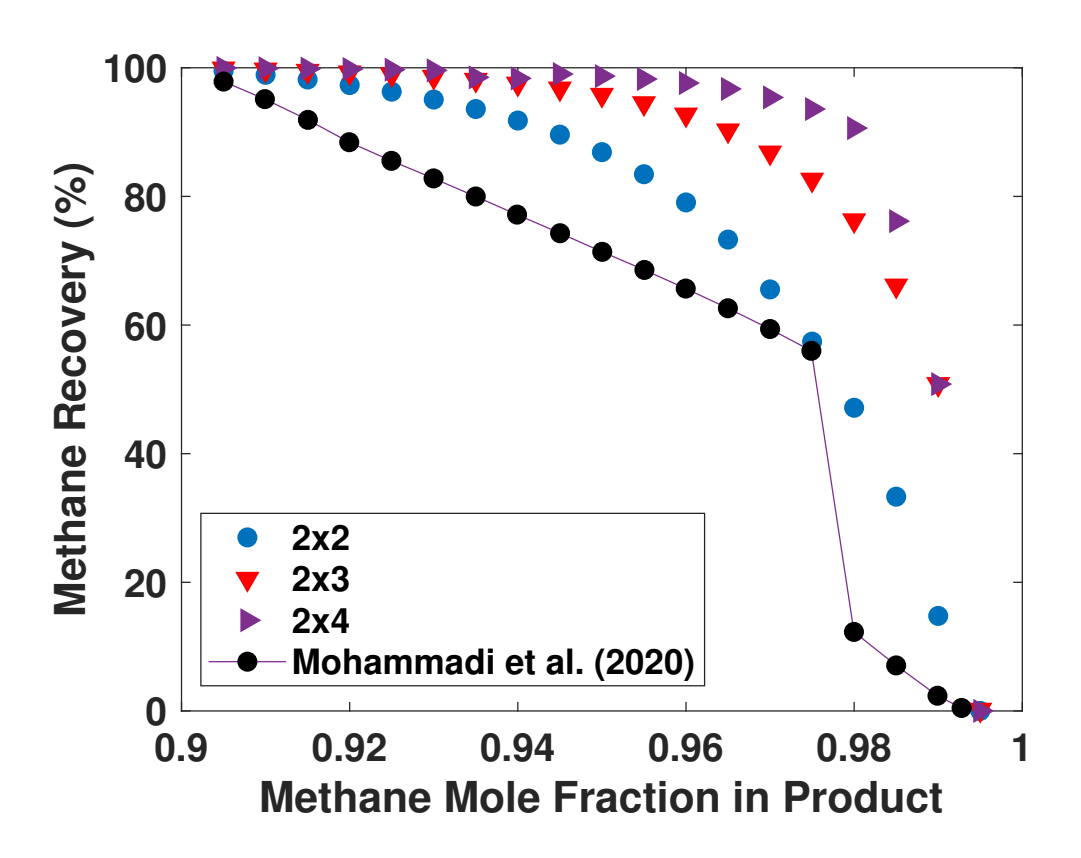


Figure 5: Multi-objective optimization results for  $\mathrm{CH}_4$  recovery from natural gas with different building block superstructure sizes.

can argue that the allowing for higher membrane areas might be the reason for this increase in the recovery. Although the reference study do not mention any specific bound on the membrane areas, we choose an upper bound on the total membrane area as 9968.59 m<sup>2</sup> which is the total membrane area of the base-case solution. When we solve the problem with

this constraint (i.e.  $\sum_{i,j,(s,m)\in SM}\left[A_{i,j,s,m}^R+A_{i,j,s,m}^F\right]\leq 9968.59$ ), we still obtain a better solution than the base-case as shown in Figure 4d with more than 73% recovery. The resulting process suggests a sweep gas flow for the first membrane. This stream is from the permeate side of the second membrane module and it is leaner  $N_2$ . This decreases the  $N_2$  composition in the permeate and increases the driving force for separation. Although we did not assume any configuration beforehand, building block-based method automatically identifies that the use of this stream as sweep gas can improve recovery. In overall, this membrane module suggests about 3% higher recovery than the already optimized base-case result.

Next, we address the same problem while accounting for the trade-offs between recovery and purity. We use  $\epsilon$ -constraint method and choose the recovery as the primary objective and use purity as the constraint in the objective problem. We use in total 19 different purity constraints starting with 90.5% and increasing with 0.5% intervals and solve each problem with building block superstructure. Furthermore, to observe the effect of number of blocks used in the solution, we also solve the same problem with different building block superstructure sizes. In total, we consider 3 different building block superstructures. The smallest structure includes  $2\times 2$  blocks allowing at most two membrane modules and the largest structure includes  $2\times4$  blocks allowing at most 4 membrane modules. We solve these problems with BARON and the resulting pareto solutions are shown in Figure 5. The pareto curve suggested by Mohammadi et al. (2020) with two membrane modules is also shown in Figure 5. The better membrane processes are located towards the upper right corner of the pareto space suggesting both high recovery and purity. The pareto curve obtained with  $2\times2$ building bock superstructure suggests much better performance at all purity levels than the reference one. Furthermore, the reference pareto curve suggests a disjoint region between 97.5%-98% purity while this is not the case for the building block superstructure result. For instance, for 98% purity, the reference optimal solution yields an optimal process with approximately 20% recovery, while the building block result suggests a process with about 50% recovery nearly 2.5 times higher than the reference solution. This indicates the utility of the building block superstructure in generation of optimal membrane-based processes.

The effect of building block superstructure size can be also observed from Figure 5. As we use more building blocks, we allow more number of membrane modules which clearly increases the performance of the corresponding membrane-based processes. However, the improvement is less pronounced towards the lower purity targets. Furthermore, the pareto curves become less apart as we use higher number of building blocks. This can be observed from the difference between the pareto fronts obtained with the  $2\times3$  and  $2\times4$  superstructures. This shows that while higher number building blocks can result in processes with better performance, the improvement demonstrates an asymptotic behavior.

Note that we did not consider the economics as the optimization objective in this case study as it is the case in the reference work. The reported solutions reveal the ultimate separation performance of the membrane materials within the specified process constraints. If one considers economics as the objective, the best solution would be different as there are also trade-offs between the process performance, operating and capital costs. Higher membrane areas result in better performance at the expense of higher capital investment. Similarly, we show that the permeate to retentate recycles increase the performance. Yet these streams require compression due to difference in pressures and they increase the operating costs. We consider these trade-offs in the remaining case studies by using economics in the objective function.

## 4.2 Application to Vapor Permeation Membrane Systems

In this case study, a literature example on methanol/water separation system will be used to demonstrate the optimal synthesis of vapor permeation membranes via building block superstructure. Luyben (2005) investigated the pressure-swing and extractive distillation processes for methanol recovery in TAME production process and found that extractive distillation is more favorable.<sup>57</sup> In that work, a distillation column is utilized to separate methanol/water mixture for methanol recovery. Here, this design will be considered as a

base-case and the potential savings from deployment of a vapor permeation membrane will be investigated. Following assumptions are made for the modeling. Membrane permeance and selectivity data are assumed to be independent of concentration, temperature and pressure. Isothermal membrane operation with counter-current flow pattern is assumed for the vapor permeation module. Pressure drop through the membrane modules are assumed negligible. Concentration polarization is neglected. Countercurrent operation for the VP membrane is assumed.

First, the distillation column design proposed by the reference is optimized as a benchmark for the membrane-based process. The feed location and number of stages are taken as the same with the original work. Optimization is performed by using the building block representation and optimization model while using the Wilson activity coefficient model to describe liquid phase nonideality. The model and superstructure representation is similar to the one used in Demirel et al. (2020)<sup>58</sup> for reactive distillation columns. The resulting optimal design has an operating cost of \$2.590 MM/year with \$2.490 MM/year hot and \$0.110 MM/year cold utility costs. This cost will serve as a target for the membrane-based process. If we can achieve any savings compared to this annual cost, then the retrofitting with membrane unit can be considered as a viable alternative.

Membrane-based process is investigated through the building block superstructure given in Figure 6. NaA zeolite is chosen as the membrane material with the permeance data obtained from the literature.<sup>59</sup> This zeolite material is highly selective towards water. A block superstructure of size  $23 \times 2$  is used. Membrane representation is similar to the one given in Figure 2b, yet, here 20 blocks are used to represent the membrane module. Complete mixing is assumed for both the permeate and retentate side blocks. As the feed mixture is in liquid state, a feed heater is considered to vaporize the feed in block  $B_{1,1}$ . This vapor mixture then can be compressed to higher pressures to increase the driving force within the membrane module. Note that use of this compressor is optional. After this compressor, a cooler option is also provided to cool down the feed if the compressor outlet temperature

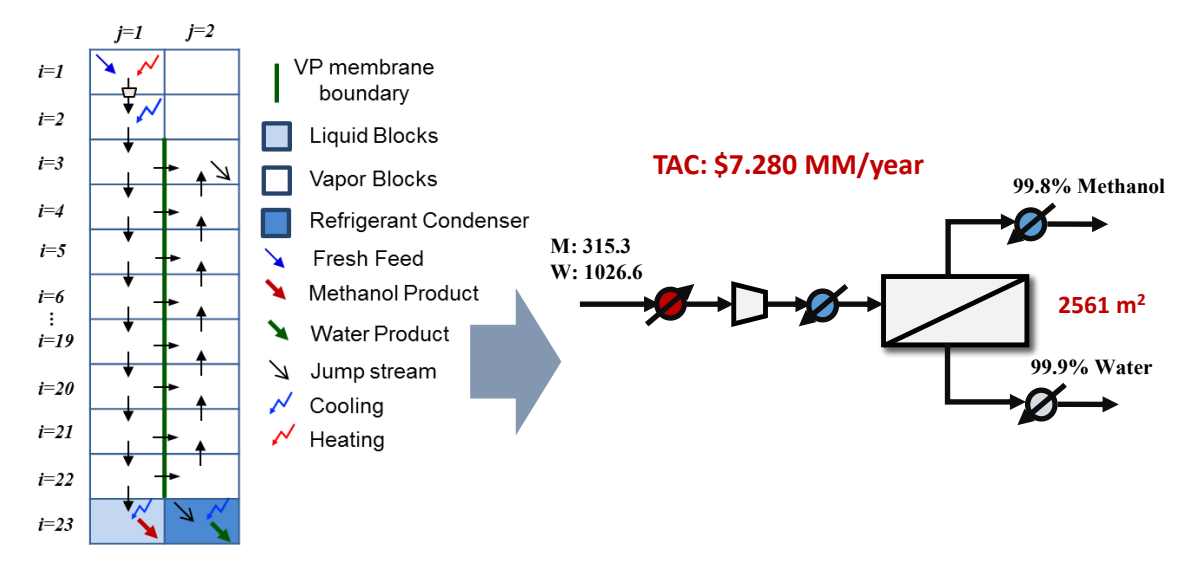


Figure 6: Standalone vapor permeation membrane solution for methanol/water separation. Figure on the left is the building block representation for the membrane module and the figure on the right is the corresponding optimal membrane process.

is above the membrane operating temperature. Furthermore, although mostly neglected in the literature, vapor permeation operations yield permeate and retentate products in vapor state which need to be condensed before they can be sent to the other parts of the process or storage units. As the permeate side is mostly operated under vacuum conditions, condensation of the permeate outlet generally requires refrigerants or brine solutions. Here, we consider a refrigerant at 263 K for the permeate condenser. High purity methanol mixture can be taken out as the retentate outlet from block  $B_{23,1}$  and high purity water mixture can be taken out from  $B_{23,2}$ . We optimize this membrane process while minimizing the TAC by considering capital investment costs for the membranes, heaters/coolers and compressors. Annualization factor of 0.2 is used for TAC calculation. Problem contains 3875 variables, 1185 constraints, 6356 non-zero elements. Optimal membrane result is shown in Figure 6. This standalone membrane unit incurs a TAC of \$7.280 MM/year. While the annualized investment cost accounts for \$1.260 MM/year, total operating costs are \$6.020 MM/year. Comparison with the operating cost of the distillation column shows that standalone membrane module with NaA zeolite is not favorable for retrofitting. It should be noted that, we only investigated a single module design. If multiple modules or hybrid

#### 4.3 Gas Permeation Membrane Network for Syngas Separation

The benefits of using building block superstructure for different process network problems is shown here via an example problem on gas permeation networks taken from Uppaluri et al. (2004). 42 In that work, an optimization framework for gas separation membrane networks was presented. The framework uses a superstructure-based optimization approach and considers different membrane flow patterns with several recycle and compression options. The building block representation of the superstructure proposed by the literature work was shown on Figure 3b. The process in the example problem is used to recover 90% of the H<sub>2</sub> with 99% purity from a syngas mixture (75% H<sub>2</sub>, 25% CO). The optimal process reported in the reference study achieves 1,624,000 \$/year total annual cost in which all membranes have counter-current flow pattern. Membranes are modeled with 10 compartments ( $n^{com} = 10$ ) and a total of 3 modules ( $n^{module} = 3$ ) are utilized. Hence, a superstructure of size  $2 \times 38$ is needed to address the same problem with building block superstructure as described in Section 2. However, we can further decrease the superstructure size if we use the last block of the membrane modules as the splitter blocks and eliminate the product mixer and splitter blocks. This yields a more compact superstructure with  $2 \times 33$  block superstructure size (Figure 7). Note that complete mixing is assumed for both the permeate and retentate side blocks similar to the reference work.

Now, we address the solution of the membrane network synthesis problem with building block superstructure. Objective function includes the investment cost for the membrane modules, recycle compressors and the operating cost associated with the electricity required for compression. Membrane property data are taken from the literature work <sup>42</sup> and provided in Table 1. Economic parameters for TAC calculation are also taken as the same with the reference work. <sup>42</sup>

In the reference work, the solution for different flow patterns are obtained separately and

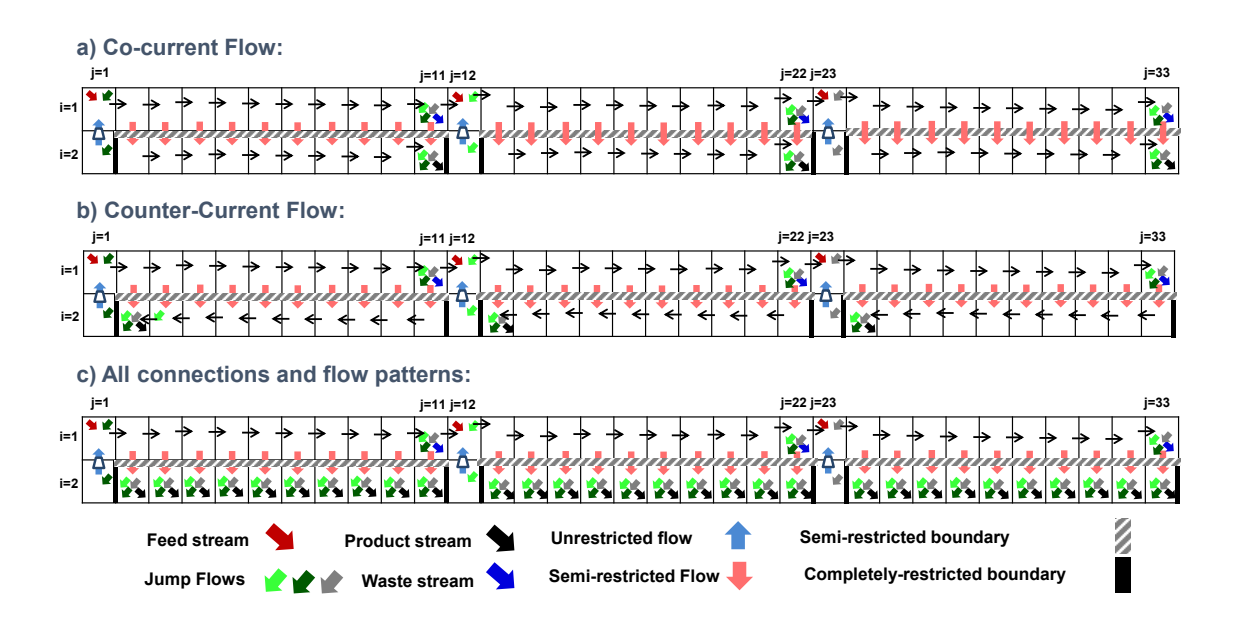


Figure 7: Different flow patterns with building block superstructure for the case study taken from Uppaluri et al. (2004).<sup>42</sup>

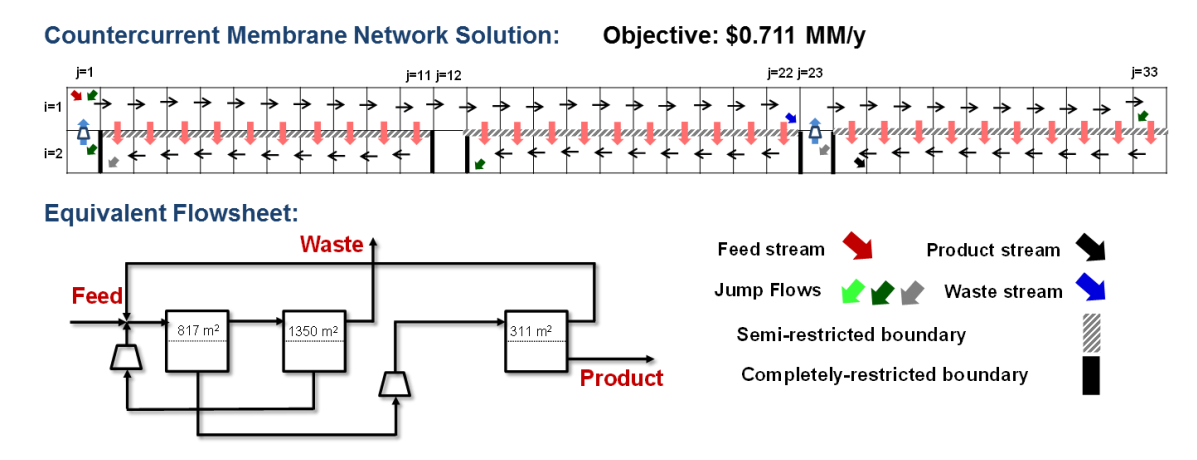


Figure 8: Solution of the membrane network synthesis problem with counter-current flow pattern.

the best solution corresponds to a counter-current membrane network. We also first solve the problem with counter-current flow pattern with the superstructure shown in Figure 7b. Problem contains 2521 continuous variables, 4281 constraints, 13524 non-zero elements. The solution of the problem with ANTIGONE yields a membrane network with \$0.711 MM/year as given in Figure 8. This network has 56% less cost than the reference case. Instead of one as in the reference solution, it has two permeate to retentate recycle streams. One of

the major reasons that we obtain much better solution is related with the solution method. While the reference study utilized stochastic optimization with simulated annealing,<sup>42</sup> we utilized a state-of-the-art MINLP solver BARON.

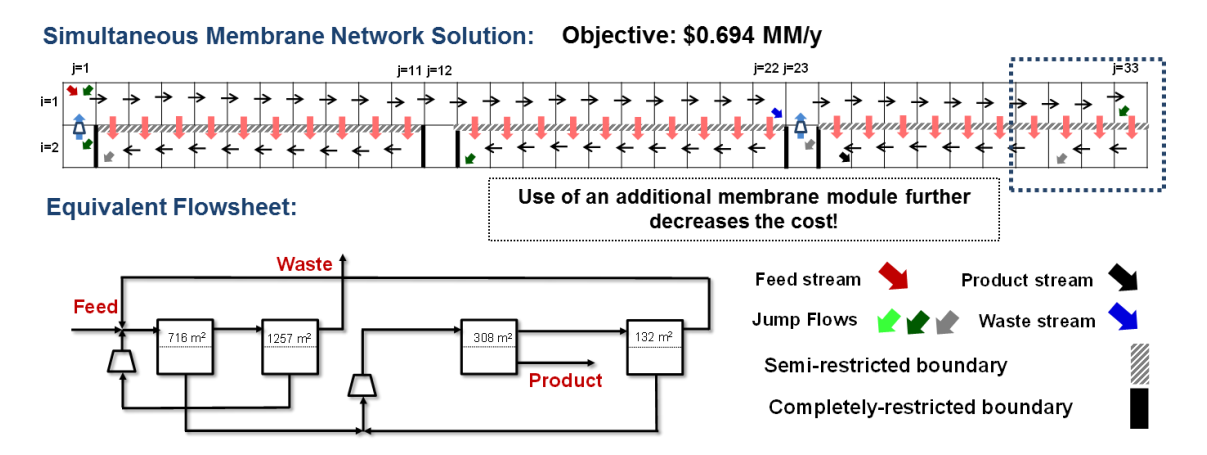


Figure 9: Solution of the membrane network synthesis problem with simultaneous consideration of all flow patterns.

While we can use the building block superstructure to address specific flow patterns separately, it can be also used for determination of the flow patterns automatically as is shown in Figure 7c. Here, all the jump stream connections are active at each block to consider cross-flow. Unlike the superstructures for the cocurrent and counter-current flow patterns, the stream directions in the permeate sides becomes variable. If the solution yields a counter-current pattern, flows will be aligned in the reverse direction to the retentate side streams. If it results in co-current pattern, flows will be aligned in the same direction with the retentate side streams. And, if the solution yields cross-flow pattern, all the interblock streams in the retentate side will have zero flows. Next, we address the same problem by using the superstructure representation while considering different flow patterns simultaneously as shown in Figure 7c. Although the problem size increases drastically due to the increase in the number of active jump streams, we use the previous countercurrent solution as an initial solution for the problem. Now, problem contains 2683 variables (32 binary variables), 4443 constraints, 14864 non-zero elements. The solution of the problem vields the block superstructure and a corresponding membrane network result as shown in

Figure 9. This network has a TAC of 0.694 MM/year with 57% improvement in TAC compared to the reference solution and 2% improvement compared to the countercurrent network solution with the building block superstructure. Interestingly, this network also utilizes counter-current flow pattern, yet we observe from the building block superstructure result that there is a discontinuity in the interblock streams within the permeate region of the third membrane module. Specifically, flow through the right boundary of the block  $B_{2,30}$  has a zero flow. This discontinuity results in two separate membrane regions and indicates an additional membrane module. With this additional module a network with lower TAC is obtained. Although we did not specify the existence of such structure beforehand, considering all flow patterns simultaneously enabled us to come up with such an improved solution. This highlights the use of building block approach as a powerful tool for superstructure-based process synthesis problems.

Table 1: Membrane network synthesis problem data. 42

Permeate pressure (bar)	10
Retentate Pressure (bar)	22
$H_2$ Permeance (kmol/m <sup>2</sup> .s.bar)	$4.689 \times 10^{-6}$
CO Permeance (kmol/m <sup>2</sup> .s.bar)	$3.125 \times 10^{-7}$
Feed Flow rate (kmol/s)	$0.0225~(75\%~\mathrm{H_2})$

#### 5 Conclusions

Membrane-based processes can offer significant benefits in terms of economics and sustainability and they bare the potential to replace more energy-intensive adsorption and distillation-based separation processes. In this work, a new optimization-based framework was introduced for the automated design, optimization, intensification, benchmarking, and technoeconomic analysis of various types of membrane systems, including gas separation, pervaporation and vapor permeation towards exploring the benefits and limits of the membrane-based solutions. The methodology is based on building block-based representation which emulates different membrane operations in a two dimensional grid formation.

This allows a generic representation method that can capture various flow patterns, membrane types and novel module designs. An MINLP-type optimization model was introduced describing the representation. The method was demonstrated on several literature problems and substantially better solutions were found compared to the best available solutions. This shows the utility of the proposed method in providing an automated design approach for various types of membrane systems, and a generic representation method for superstructure-based synthesis of membrane separation processes. Future work will be performed to enrich the proposed framework with reactive and hybrid membrane-based processes.

#### Acknowledgments

The authors gratefully acknowledge support from the NSF CAREER award CBET-1943479, and the DOE RAPID Institute SYNOPSIS Project (DE-EE0007888-09-03). Salih Emre Demirel acknowledges Texas A&M Energy Institute Fellowship.

### **Supporting Information**

Energy flow constraints. This information is available free of charge via the Internet at http://pubs.acs.org.

### References

- Sholl, D. S.; Lively, R. P. Seven chemical separations to change the world. Nature 2016, 532, 435–437.
- 2. Burns, R. L.; Koros, W. J. Defining the challenges for C3H6/C3H8 separation using polymeric membranes. *Journal of Membrane Science* **2003**, *211*, 299–309.
- Khalilpour, R.; Mumford, K.; Zhai, H.; Abbas, A.; Stevens, G.; Rubin, E. S. Membrane-based carbon capture from flue gas: a review. *Journal of Cleaner Production* 2015, 103, 286–300.
- 4. Scholes, C. A.; Stevens, G. W.; Kentish, S. E. Membrane gas separation applications in natural gas processing. *Fuel* **2012**, *96*, 15–28.
- 5. Baker, R. W. Membrane technology and applications; John Wiley & Sons, 2012.
- 6. Scott, K. Handbook of industrial membranes; Elsevier, 1995.
- 7. Koros, W. J.; Mahajan, R. Pushing the limits on possibilities for large scale gas separation: which strategies? *Journal of Membrane Science* **2000**, *175*, 181–196.
- 8. Huang, H.-J.; Ramaswamy, S.; Tschirner, U. W.; Ramarao, B. A review of separation technologies in current and future biorefineries. *Separation and purification technology* **2008**, *62*, 1–21.
- 9. Drioli, E.; Stankiewicz, A. I.; Macedonio, F. Membrane engineering in process intensification—An overview. *Journal of Membrane Science* **2011**, *380*, 1–8.
- 10. Morigami, Y.; Kondo, M.; Abe, J.; Kita, H.; Okamoto, K. The first large-scale pervaporation plant using tubular-type module with zeolite NaA membrane. Separation and Purification Technology 2001, 25, 251–260.

- 11. Kee, R. J.; Karakaya, C.; Zhu, H. Process intensification in the catalytic conversion of natural gas to fuels and chemicals. *Proceedings of the Combustion Institute* **2017**, *36*, 51–76.
- 12. Bose, S.; Kuila, T.; Nguyen, T. X. H.; Kim, N. H.; Lau, K.-t.; Lee, J. H. Polymer membranes for high temperature proton exchange membrane fuel cell: recent advances and challenges. *Progress in Polymer Science* **2011**, *36*, 813–843.
- 13. Shao, Y.; Zavala, V. M. Modularity measures: Concepts, computation, and applications to manufacturing systems. *AIChE Journal* **2020**, *66*, e16965.
- 14. Stankiewicz, A. I.; Moulijn, J. A. Process intensification: transforming chemical engineering. *Chemical engineering progress* **2000**, *96*, 22–34.
- 15. Bielenberg, J.; Bryner, M. Realize the potential of process intensification. *Chemical Engineering Progress* **2018**, *114*, 41–45.
- 16. Drioli, E.; Curcio, E. Membrane engineering for process intensification: a perspective.

  Journal of Chemical Technology & Biotechnology: International Research in Process,

  Environmental & Clean Technology 2007, 82, 223–227.
- 17. Tian, Y.; Demirel, S. E.; ; Hasan, M. M. F.; Pistikopoulos, E. N. An Overview of Process Systems Engineering Approaches for Process Intensification: State of the Art. *Chemical Engineering and Processing: Process Intensification* **2018**, 133, 160 210.
- 18. Demirel, S. E.; Li, J.; Hasan, M. F. Systematic process intensification. *Current Opinion in Chemical Engineering* **2019**, *22*, 108–113.
- Carrasco, J. C.; Lima, F. V. Novel operability-based approach for process design and intensification: Application to a membrane reactor for direct methane aromatization. AIChE Journal 2017, 63, 975–983.

- 20. Bishop, B. A.; Lima, F. V. Modeling, Simulation, and Operability Analysis of a Nonisothermal, Countercurrent, Polymer Membrane Reactor. *Processes* **2020**, *8*, 78.
- 21. Abetz, V.; Brinkmann, T.; Dijkstra, M.; Ebert, K.; Fritsch, D.; Ohlrogge, K.; Paul, D.; Peinemann, K.-V.; Pereira-Nunes, S.; Scharnagl, N.; Schossig, M. Developments in membrane research: from material via process design to industrial application. Advanced Engineering Materials 2006, 8, 328–358.
- Drioli, E.; Giorno, L. Comprehensive membrane science and engineering; Newnes, 2010;
   Vol. 1.
- 23. Babi, D. K.; Lutze, P.; Woodley, J. M.; Gani, R. A process synthesis-intensification framework for the development of sustainable membrane-based operations. *Chemical Engineering and Processing: Process Intensification* 2014, 86, 173–195.
- 24. Ahmad, F.; Lau, K. K.; Shariff, A. M.; Murshid, G. Process simulation and optimal design of membrane separation system for CO2 capture from natural gas. *Computers & Chemical Engineering* **2012**, *36*, 119–128.
- 25. Hasan, M. F.; Baliban, R. C.; Elia, J. A.; Floudas, C. A. Modeling, simulation, and optimization of postcombustion CO<sub>2</sub> capture for variable feed concentration and flow rate. 1. Chemical absorption and membrane processes. *Industrial & Engineering Chemistry Research* 2012, 51, 15642–15664.
- Guan, G.; Yang, X.; Wang, R.; Field, R.; Fane, A. G. Evaluation of hollow fiber-based direct contact and vacuum membrane distillation systems using aspen process simulation.
   Journal of Membrane Science 2014, 464, 127–139.
- 27. Lutze, P.; Gorak, A. Reactive and membrane-assisted distillation: Recent developments and perspective. *Chemical engineering research and design* **2013**, *91*, 1978–1997.

- He, X.; Kumakiri, I.; Hillestad, M. Conceptual Process Design and Simulation of Membrane Systems for Integrated Natural Gas Dehydration and Sweetening. Separation and Purification Technology 2020, 116993.
- DeJaco, R. F.; Loprete, K.; Pennisi, K.; Majumdar, S.; Siepmann, J. I.; Daoutidis, P.;
   Murnen, H. K.; Tsapatsis, M. Modeling and Simulation of Gas Separations with
   Spiral-Wound Membranes. AIChE Journal 2020, 66, e16274.
- 30. Castoldi, M. T.; Pinto, J. C.; Melo, P. A. Modeling of the separation of propene/propane mixtures by permeation through membranes in a polymerization system. *Industrial & engineering chemistry research* **2007**, *46*, 1259–1269.
- 31. Rall, D.; Schweidtmann, A. M.; Kruse, M.; Evdochenko, E.; Mitsos, A.; Wessling, M. Multi-scale membrane process optimization with high-fidelity ion transport models through machine learning. *Journal of Membrane Science* **2020**, 118208.
- 32. Marriott, J.; Sørensen, E.; Bogle, I. Detailed mathematical modelling of membrane modules. Computers & Chemical Engineering 2001, 25, 693–700.
- 33. Tessendorf, S.; Gani, R.; Michelsen, M. L. Modeling, simulation and optimization of membrane-based gas separation systems. *Chemical engineering science* **1999**, *54*, 943–955.
- 34. Pathare, R.; Agrawal, R. Design of membrane cascades for gas separation. *Journal of membrane science* **2010**, *364*, 263–277.
- 35. Zarca, R.; Ortiz, A.; Gorri, D.; Biegler, L. T.; Ortiz, I. Optimization of multistage olefin/paraffin membrane separation processes through rigorous modeling. *AIChE Journal* **2019**, *65*, e16588.
- 36. Aliaga-Vicente, A.; Caballero, J. A.; Fernández-Torres, M. J. Synthesis and optimization

- of membrane cascade for gas separation via mixed-integer nonlinear programming. AIChE Journal 2017, 63, 1989–2006.
- 37. Ohs, B.; Lohaus, J.; Wessling, M. Optimization of membrane based nitrogen removal from natural gas. *Journal of Membrane Science* **2016**, *498*, 291–301.
- 38. Eugene, E. A.; Phillip, W. A.; Dowling, A. W. Computer Aided Chemical Engineering; Elsevier, 2019; Vol. 47; pp 469–474.
- 39. Eugene, E.; Phillip, W.; Dowling, A. Material property targets for emerging nanomaterials to enable point-of-use and point-of-entry water treatment systems. **2020**,
- 40. Kim, J. F.; da Silva, A. M. F.; Valtcheva, I. B.; Livingston, A. G. When the membrane is not enough: A simplified membrane cascade using Organic Solvent Nanofiltration (OSN). Separation and Purification Technology 2013, 116, 277–286.
- 41. Arias, A. M.; Mussati, M. C.; Mores, P. L.; Scenna, N. J.; Caballero, J. A.; Mussati, S. F. Optimization of multi-stage membrane systems for CO2 capture from flue gas. *International Journal of Greenhouse Gas Control* 2016, 53, 371–390.
- 42. Uppaluri, R. V.; Linke, P.; Kokossis, A. C. Synthesis and optimization of gas permeation membrane networks. *Industrial & engineering chemistry research* **2004**, *43*, 4305–4322.
- 43. El-Halwagi, M. M.; Manousiouthakis, V. Synthesis of mass exchange networks. *AIChE Journal* **1989**, *35*, 1233–1244.
- 44. Srinivas, B.; El-Halwagi, M. Optimal design of pervaporation systems for waste reduction. *Computers & chemical engineering* **1993**, *17*, 957–970.
- 45. Bounaceur, R.; Berger, E.; Pfister, M.; Santos, A. A. R.; Favre, E. Rigorous variable permeability modelling and process simulation for the design of polymeric membrane gas separation units: MEMSIC simulation tool. *Journal of membrane science* **2017**, 523, 77–91.

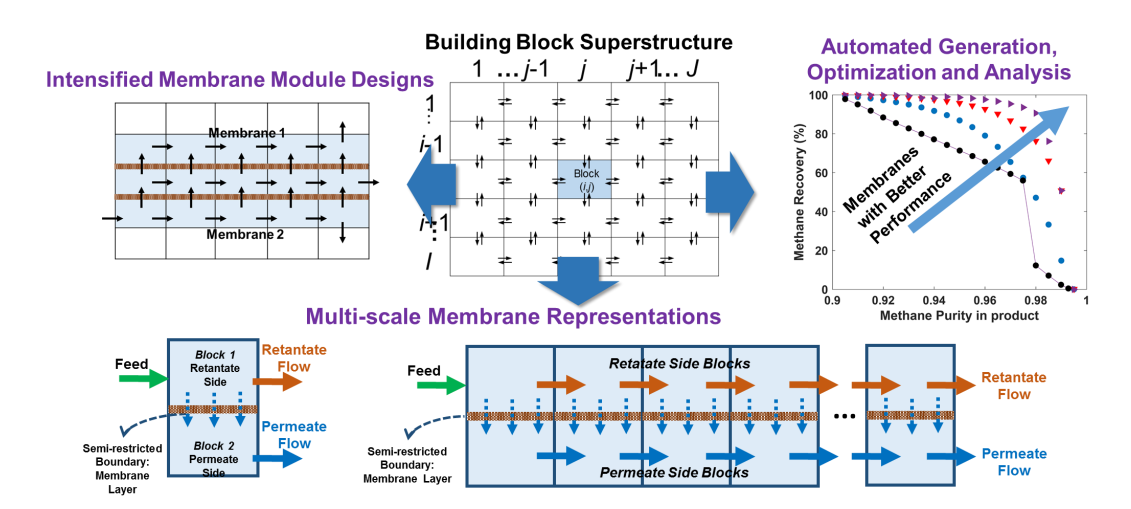
- 46. Mohammadi, Y.; Matsuura, T.; Jansen, J. C.; Esposito, E.; Fuoco, A.; Dumée, L. F.; Gallucci, F.; Drioli, E.; Soroush, M. Optimal Membrane-Process Design (OMPD): A software product for optimal design of membrane gas separation processes. Computers & Chemical Engineering 2020, 135, 106724.
- 47. Mencarelli, L.; Chen, Q.; Pagot, A.; Grossmann, I. E. A review on superstructure optimization approaches in process system engineering. *Computers & Chemical Engineering* **2020**, 106808.
- 48. Tula, A. K.; Eden, M. R.; Gani, R. Computer-aided process intensification: Challenges, trends and opportunities. *AIChE J* **2019**, *66*, e16819.
- 49. Demirel, S. E.; Li, J.; Hasan, M. M. F. Systematic process intensification using building blocks. *Computers & Chemical Engineering* **2017**, *105*, 2–38.
- 50. Demirel, S. E.; Li, J.; Hasan, M. F. A general framework for process synthesis, integration, and intensification. *Industrial & Engineering Chemistry Research* **2019**, *58*, 5950–5967.
- 51. Hasan, M.; Demirel, S. E.; Li, J. A Building Block Approach to Process Intensification.

  Chemical Engineering Progress 2019, 115, 35–43.
- 52. Li, J.; Demirel, S. E.; Hasan, M. M. F. Process Synthesis using a Block Superstructure with Automated Flowsheet Generation and Optimization. AIChE Journal 2018, 64, 3082–3100.
- 53. Li, J.; Demirel, S. E.; Hasan, M. F. Computer Aided Chemical Engineering; Elsevier, 2019; Vol. 47; pp 421–426.
- 54. Li, J.; Demirel, S. E.; Hasan, M. M. F. Process Integration Using Block Superstructure.

  Industrial & Engineering Chemistry Research 2018, 57, 4377–4398.

- 55. Iyer, S. S.; Demirel, S. E.; Hasan, M. F. Combined natural gas separation and storage based on in silico material screening and process optimization. *Industrial & Engineering Chemistry Research* **2018**, *57*, 16727–16750.
- 56. Lokhandwala, K. A.; Pinnau, I.; He, Z.; Amo, K. D.; DaCosta, A. R.; Wijmans, J. G.; Baker, R. W. Membrane separation of nitrogen from natural gas: a case study from membrane synthesis to commercial deployment. *Journal of Membrane Science* 2010, 346, 270–279.
- 57. Luyben, W. L. Comparison of pressure-swing and extractive-distillation methods for methanol-recovery systems in the TAME reactive-distillation process. *Industrial & engineering chemistry research* **2005**, *44*, 5715–5725.
- 58. Demirel, S. E.; Li, J.; El-Halwagi, M.; Hasan, M. F. Sustainable Process Intensification Using Building Blocks. ACS Sustainable Chemistry & Engineering 2020, 8, 17664–17679.
- 59. Okamoto, K.-i.; Kita, H.; Horii, K.; Kondo, K. T. Zeolite NaA membrane: preparation, single-gas permeation, and pervaporation and vapor permeation of water/organic liquid mixtures. *Industrial & engineering chemistry research* **2001**, *40*, 163–175.
- 60. Tula, A. K.; Befort, B.; Garg, N.; Camarda, K. V.; Gani, R. Sustainable process design & analysis of hybrid separations. *Computers & Chemical Engineering* **2017**, *105*, 96–104.

# **TOC** Graphic



For Table of Contents Use Only